*Journal of The Electrochemical Society*, 2023 **170** 020509
1945-7111/2023/170(2)/020509/19/$40.00 © 2023 The Electrochemical Society ("ECS"). Published on behalf of ECS by IOP Publishing Limited

# Electrodeposition of Li-Ion Cathode Materials: The Fascinating Alternative for Li-Ion Micro-Batteries Fabrication

**Sepideh Behboudikhiavi, Joel Ojonugwa Omale, Binson Babu, Luc Piraux, and Alexandru Vlad**[z]

*Institute of Condensed Matter and Nanosciences, Université Catholique de Louvain, Louvain-la-Neuve, Belgium*

Li-ion microbatteries are the frontline candidates to fulfill the requirements of powering miniature autonomous devices. However, it still remains challenging to attain the required energy densities of $> 0.3$mWh cm$^{-2}$ $\mu$m$^{-1}$ in a planar configuration. To overcome this limitation, 3D architectures of LIMBs have been proposed. However, most deposition techniques are poorly compatible with 3D architectures because they limit the choice of current collectors and selective deposition of the active materials. Electrodeposition was suggested as an alternative for rapidly and reproducibly depositing active materials under mild conditions, and with controlled properties. However, despite the huge potential, electrodeposition remains underexplored for LIMB cathode materials, partly due to challenges associated with the electrodeposition of Li-ion phases. Herein, we review advances in the electrodeposition of Li-ion cathode materials with the main focus set on the direct, one-step deposition of electrochemically active phases. We highlight the merits of electrodeposition over other methods and discuss the various classes of reported materials, including layered transition metal oxides, vanadates, spinel, and olivines. We offer a perspective on the future advances for the adoption of electrodeposition processes for the fabrication of microbatteries to pave the way for future research on the electrodeposition of cathode materials.
 [DOI: 10.1149/1945-7111/acb6b9]

Manuscript submitted August 21, 2022; revised manuscript received October 31, 2022. Published February 8, 2023.

*Review*

# Electrodeposition of Li-ion cathode materials: the fascinating alternative for Li-ion micro-batteries fabrication

Sepideh Behboudikhiavi, Joel Ojonugwa Omale, Binson Babu, Luc Piraux and Alexandru Vlad[z]

Institute of Condensed Matter and Nanosciences, Université Catholique de Louvain, Louvain-la-Neuve, Belgium.

## Abstract

Li-ion microbatteries are the frontline candidates to fulfill the requirements of powering miniature autonomous devices. However, it still remains challenging to attain the required energy densities of > 0.3mWh/cm$^{-2}$µm$^{-1}$ in a planar configuration. To overcome this limitation, 3D architectures of LIMBs have been proposed. However, most deposition techniques are poorly compatible with 3D architectures because they limit the choice of current collectors and selective deposition of the active materials. Electrodeposition was suggested as an alternative for rapidly and reproducibly depositing active materials under mild conditions, and with controlled properties. However, despite the huge potential, electrodeposition remains underexplored for LIMB cathode materials, partly due to challenges associated with the electrodeposition of Li-ion phases. Herein, we review advances in the electrodeposition of Li-ion cathode materials with the main focus set on the direct, one-step deposition of electrochemically active phases. We highlight the merits of electrodeposition over other methods and discuss the various classes of reported materials, including layered transition metal oxides, vanadates, spinel, and olivines. We offer a perspective on the future advances for the adoption of electrodeposition processes for the fabrication of microbatteries to pave the way for future research on the electrodeposition of cathode materials.

## Introduction

Lithium-ion batteries (LIBs) are the game-changing energy storage technology of the 21$^{st}$ century.[1–4] Besides the large-scale applications of LIBs for renewable energy storage and electric transportation, Li-ion microbatteries (LIMBs) have emerged as promising power sources for autonomous miniaturized microelectronic devices, e.g., medical implants, micro-sensors, self-powered integrated circuits, microelectromechanical systems, and the plethora of devices associated with the Internet-of-Things (IoT).[5–10] However, the developments in LIMBs have not kept pace with the fast and ever-growing developments in microelectronics. Therefore, further developments in miniaturized electronic devices and IoT seem dependent on the maturing of LIMB technology to meet the specifications for high energy and power densities.[11,12] Essentially, these features should be provided by small-size LIMBs, i.e., < 10 mm$^3$, in addition to stable and safe cycling performances.[11–14] To fulfill these requirements, rapid advances in both cell design and electrode chemistry are required. Regarding cell design, both the configuration and electrode architecture play critical roles in meeting the specifications of LIMBs. While the areal capacity of an electrode is proportional to the mass loading (mass per unit area), hence the thickness, of the active electrode materials $Q \sim l$ (where $Q$ is the electrode capacity and $l$ is the electrode thickness), the areal power capability scales according to $p \sim \tau^{-1} \sim D/l^2$ (where $p$ is the power capability, $\tau$ is the Li diffusion time, $l$ is the electrode thickness, and $D$ is the Li diffusion coefficient). These antithetical design rules impose a limitation on simultaneously increasing the areal capacity and power capabilities of microbatteries.[3,15]

Based on the cell configuration and electrode architecture, LIMBs can be categorized into two main classes: 2D and 3D electrode design LIMBs.[13,16,17] The 2D configuration is the most widely adopted LIMB configuration; it refers to a LIMB with stacked thin-film electrodes separated by an electrolyte.[18] The 2D LIMBs have outstanding power capabilities when the electrodes have small thicknesses, but their high power capability come at the cost of limited areal energy density and capacity. To decouple the power capability and energy of LIMBs, the 3D configuration has been actively pursued as an alternative to increasing the areal energy and power capability of LIMBs simultaneously (Fig. 1a).[12,16,19,20]

[z] alexandru.vlad@uclouvain.be

3D LIMBs refer to microbatteries whose current collectors and/or individual electrodes have 3D geometries (Figs. 1a and 1b).[21] The possible 3D configurations used for microbatteries include interdigitated, trench, concentric, and aperiodic configurations (Fig. 1b). [19,21,22] These 3D architectures facilitate faster transport of electrons and ions, leading to high power capabilities, without limiting the possibility to increase the mass loading and hence the areal capacity.

Conformal thin-film coating of 3D current collectors with active materials is an attractive strategy to accomplish high power capability and energy density for LIMBs.[16,20,23] However, the technical difficulties with the deposition of Li-ion cathode materials as conformal films restrict the development of high-performance and cost-effective LIMBs. Based on the critical role of the cathode (positive electrode) materials on the energy density and cost of LIMB, their sophisticated design remains the main challenge to be addressed, regardless of the scale of the battery.[2,24]

Various chemistries have been applied as cathode materials of 3D LIMBs, including conventional Li-ion cathode materials such as $LiFePO_4$(LFP)[25], $LiMn_2O_4$(LMO)[23], $LiCoO_2$(LCO)[26], and $Li_xMnO_2$[27]. Nonetheless, compared to anode syntheses, cathode syntheses are highly challenging.[16] One of the main difficulties is that the synthesis of cathode chemistries typically requires post-annealing steps to transform the as-deposited materials to their electrochemically active phases, which increases the risk of degrading the substrate or the device. Therefore, most research on the deposition of cathode materials is limited to Li-free chemistries, such as $V_2O_5$[28], $VO_2$[29], or $FePO_4$,[30] as well as other less common chemistries such as $MoS_2$[31], CuS[32], FeS[33], polyaniline[34], and polypyrrole.[35] In this regard, the development of one-step deposition techniques of Li-containing cathode materials, with the capability of conformal deposition on 3D architectures under mild conditions is vital to acquiring high energy/power full-cell 3D LIMBs.

As shown in Fig. 1c, the most applied techniques for the fabrication of 3D LIMBs fall into the following 4 groups – 3D printing,[36,37] lithography,[28,38] liquid-phase deposition[39], and vapor-phase deposition.[41] These techniques are used alone or in combination with one another and can be used to fabricate individual electrodes, electrolytes, current collectors, and packaging. Even though the vapor-phase deposition methods (thermal evaporation,[42] radio-frequency magnetron sputtering,[43] chemical vapor deposition (CVD),[44] pulse laser deposition (PLD),[45] and atomic layer deposition (ALD)[46]) can provide conformal coatings on 3D architectures, most of them require complex and costly instrumentation and facilities.

Among the vapor-phase techniques, ALD is probably the most prosperous method to grow conformal films with the capability of precise control over the thickness and composition, particularly in the conformal coating of complex 3D nanostructures.[47] However, the impediments of this technique to growing Li-containing cathode films consist of (i) lack of lithium-containing precursors with high vapor pressure, (ii) surface-limiting interference of water as a counter reagent, (iii) undesired high mobility of $Li^+$ at high temperatures required for deposition (200-300 °C), and (iv) low deposition rates, all of these considerably diminish its attractiveness and efficiency.[3,48]

Alternatively, 3D printing has emerged as a powerful and cost-saving approach to partially address the drawbacks of other methods.[49,50] It enables the fabrication of 3D LIMBs with flexible dimensions and well-controlled geometries without the need for templates, both at the component (electrodes and current collectors) and packaging level.[20,49,51] However, 3D printing suffers from several bottlenecks such as sequential (and thus long-time) processing, coarse printing resolution (10 to 30 μm), ink stability, printing uniformity, and poor adhesion between printed films and certain substrates.[49,52] On the one hand, the possibility of only printing thick electrode layers limits the power densities of 3D-printed LIMBs; on the other hand, the fact that the printing inks consist of conducting and binding additives, in addition to the active electrode materials, decreases the areal energies of 3D-printed LIMBs by 10 – 40 %.[52,53] Moreover, these additives could cause inferior electrochemical and mechanical properties as a result of insufficient interfacial interactions with active material as well as weak adhesion to the substrate.[54] To date, LFP [36,37,49,55], LMO[49,56] as well as LCO[49,57] have been probably the most 3D printed cathode materials for LIB/LIMB. Schematic illustrations and examples of 3D-printed LFP electrodes and cells are shown in Figs. 2a-2g. Although the LIMBs comprised of 3D printed LFP/$LiTi_5O_{12}$ (LTO) electrodes exhibited high areal energy density (9.7 J $cm^{-2}$) and power density (2.7 mW $cm^{-2}$),[36] the challenges ahead of widespread utilization of this technique should not be overlooked. Furthermore, for 3D printing, limited availability of printable active materials inks and low compatibility of the applied inks with the other components (in the case of sequential printing of full batteries) are some of the main challenges, which makes 3D printing less convenient for advancing 3D LIMBs.[18]

Lithography technologies, such as holographic[38] and imprint techniques,[28] have also been utilized for the generation of 3D features in current collectors and active materials of LIMBs. These techniques have the advantage of being able to form a variety of complex 3D geometries with structural features as low as 50 nm.[38] For example, Lethien et al.[58] reported micropatterning of silicon wafers with UV photolithography via photoresist etching mask combined with a deep reactive ion etching method to obtain Si nanopillars. Then they deposited sequential layers of lithium phosphorous oxynitride (LIPON) solid electrolyte which was followed by the deposition of LFP with the use of the magnetron sputtering technique. These approaches, however, remain multistep processes, requiring long processing time and a host of parameters that need to be optimized. Furthermore, since they only form 3D features, this technology needs to be conducted in combination with vapor-phase techniques (discussed above) and liquid-phase deposition techniques such as electrodeposition (which will be exclusively referred to as ECD hereafter)[59] and electrostatic spray deposition.[28,38,39,60]

The shortcomings of the above-discussed deposition techniques unveil the importance of an alternative method for the conformal thin-film coating of LIB/LIMB cathode materials. In this regard, ECD is a well-suited technique for the synthesis of conformal defect-free thin films on complex porous surfaces with a high surface area. ECD has been exploited in coating and finishing technologies for decades.[61–64] It provides the opportunity of controlling and designing the physicochemical properties of the final

product simply by manipulating the parameters such as electrolyte chemistry and applied current/potential, allowing for the precise tuning of the crystal growth rate and orientation, surface morphology, pore size distribution, as well as deposition rate. However, the widespread application of this technique could be limited due to the several shortcomings including poor adhesion of the electrodeposit, occurrence of cracks and pinholes in the electrodeposited film as well as the necessity of using the conductive substrate.[65] The other specific challenges of the ECD technique to acquire conformal films of cathode materials could be the lack of controlling the quality of electrodeposited film on the atomic scale as well as the precise controlling of the chemical composition of electrodeposit. Regardless of the aforementioned drawbacks, the numerous advantages of this technique over the other deposition methods have triggered a big interest in ECD as a highly versatile synthesis strategy of different kinds of energy storage materials[59,66–72] and their integration into nano/micro-fabrication of the various components of LIMBs.[28,31,73,74]

The ECD technique has been explored to realize most of the LIMB constituents, including current collectors[75], cathode[76,77] solid electrolytes,[78] and anodes[79,80] while working under mild conditions and being compatible with the micro/electronic fabrication. However, despite the huge potential to produce conformal thin films on various conducting substrates, the ECD of cathode films of LIMBs remains poorly addressed.[7,81] In this regard, ECD holds the potential to benefit both LIMB and LIB in the following paramount aspects: 1) conformal ECD of cathode material directly on substrates with complex geometries, at low temperatures and ambient pressure; 2) applicable to a broad range of conductive substrates with a lightweight and large area, e.g. metal foams, carbon cloths, etc.; 3) discarding the need for additives such as binder and conductive agents with realizing binder-free electrodes, which could enable higher energy density since the whole cathode thin film is electrochemically active.[60,82] Yet, all the aforementioned benefits could be fulfilled if the whole electrochemical synthesis of cathode material would be possible in a single step, and shows comparable electrochemical performance attained by the materials synthesized through the conventional solid-state methods.[76] It is worth mentioning that there are many investigations on the ECD of Li-free cathode materials. In particular, $MnO_2$[77,83] and $V_2O_5$[84] phases have been utilized as LIMB electrodes (as discussed above), taking the advantage of their high operating potential and well-established ECD conditions. It seems that the intensive development in Li metal-based batteries and microbatteries along with solid-state electrolyte development has revived the research and development of Li-free cathode materials. These cathode materials, thanks to their low cost, environmental friendliness (of Mn-oxides phases, for instance), high energy density, and moisture tolerance, could be suitable alternatives to their Li-containing counterparts.[85] Nevertheless, incorporating these materials in full-cell LIMBs imposes additional steps of cathode pre-lithiation, employing lithiated anode materials, or the use of pure Li metal.[3] These strategies not only require extra processing steps but also need post-lithiation after the ECD, which could detrimentally affect the adherence of the deposited thin film to the underlying substrate. Therefore, it is highly desirable to develop Li-containing cathode materials through the ECD technique, which works under milder conditions, for the fabrication of 3D LIMBs.

In this work, we review the advances in direct ECD of electrochemically active Li-ion-containing cathode (positive electrode) materials with a focus on one-step ECD that does not involve any post-ECD treatment (e.g., annealing, pre-lithiation, etc). Several classes of chemistries are identified and detailed. We discuss the research on various categories of Li-containing cathode materials, including lithium transition metal oxides (LTMOs, mainly LCO, $LiNiO_2$ (LNO), $LiMnO_2$, $Li_3VO_4$/$LiV_2O_5$ (LVO)), spinel LMO as well as LFP. It is noteworthy that the literature on this subject can be categorized based on the ECD medium such as molten salt and aqueous/organic (ionic liquid). We also discuss Li-free cathode materials, including $MnO_2$, $V_2O_5$, $MoS_xO_y$, and $FeS_2$ as interesting and competitive options over Li-containing cathode materials with well-established ECD procedures, which could benefit LIMBs' fast progression. Future directions and new paradigms are also suggested to inspire research and development in this promising area considering the urgent need for developing LIMBs.

## ECD of Li-containing cathode materials in a non-aqueous medium

### ECD from molten salt electrolytes

The pioneering advance for molten salt ECD of LTMOs came from Zhang et al.[76] in 2017, wherein direct ECD of LCO, LMO, and Al-doped LCO was achieved for the first time in non-aqueous molten salt eutectic mixtures (LiOH-KOH) under relatively low-temperature (260 °C). They found that the electroplated oxides possess similar crystallinities and electrochemical performances to the powders obtained via solid-state methods that were performed at high temperatures (700° to 1000 °C). Since the used melt is a hydroxide mixture, the electroplating potential and thermodynamic stability of each compound are influenced by the acidity ($pH_2O$, which is defined as -log ($\chi_{H_2O}$) of the molten salt. In a hydroxide melt , $H_2O$ acts as a Lux-flood acid which stabilizes the equilibrium reaction ($2OH^- = H_2O + O^{2-}$) by absorbing the basic species of $O^{2-}$, and by controlling the water concentration ($\boldsymbol{\chi_{H_2O}}$), hence, changing the acidity of the melt, precipitation of the product could be controlled.[86] For instance, the potential-$pH_2O$ diagram (Pourbaix diagram) of the LiOH-KOH-CoO eutectic system (Fig. 3a), shows the possibility of ECD of LCO in hydroxide molten salt without $O_2$ evolution. Thus, the LCO was electrodeposited on various substrates such as conventional Al foil, carbon nanofiber paper, and mesoporous carbon foam, by applying a pulsed waveform (1.1 V pulse for 2 s and open-circuit potential for 2 min) between the working and the reference electrodes, where Co wire is used as a pseudo-reference electrode, and Ni plate as the counter electrode (Fig. 3b), in a near-eutectic hydroxide melt based on the following reaction, which is described in Equation 1:

$$2\,LiOH + 3\,CoO \rightarrow 2LiCoO_2 + Co + H_2O \qquad (1)$$

The electrodeposited LCO was crystalline, with an observable split of (110) and (108) peaks, evidencing the HT-O3 LCO phase (Fig. 3c), which is also corroborated by the well-defined plateaus (~3.9 V) and the sharp peaks in the dQ/dV (Fig. 3d). Further, the electroplated LCO exhibited a specific capacity of 138 mAh $g^{-1}$ between 3.0 to 4.2 V (*vs.* $Li/Li^+$), akin to the high-temperature synthesized conventional LCO. They have also demonstrated the possibilities of in situ coating of LCO with conformal morphologies, through the surface-driven ECD, on various conductive substrates such as Al foil, mesoporous carbon foam, and carbon nanofiber (CNF) scaffold, to fabricate binder-free cathodes for LIB. By controlling the deposition voltage and duty cycle during the pulsed ECD, and depending on the substrates, the ECD enables the flexibility to tune the porosity (10-60%) and thickness of the electrodes. They showed a ~25-µm-thick, ~80%-dense LCO film grown directly on the Al foil (Fig. 3e), which can be extended to ~ 200 µm in thickness, owing to the excellent electrical conductivity of the electrodeposited LCO film.

Besides, they have also demonstrated the ECD of high crystalline spinel LMO on a 3D CNF scaffold, by using LiOH-KOH-MnO eutectic mixture melt, and Al-doped LCO, by adding $Al(OH)_3$ to the LiOH-KOH-CoO eutectic mixture melt. This demonstrates the generality of the utilization of LiOH-KOH near-eutectic melt in ECD of LTMO, which is attributed to the melt's high dissolving power of transition metal oxides at relatively low temperature (~200 °C) and higher stability over a relatively large potential window.

Ates et al.[87] patented the possibility of ECD of LTMOs using a modified method, through low purity starting precursors based on the reported procedure by Zhang et al.[76] In this study, the molten salt was prepared with KOH and various Li precursors with lower purity (e.g. LiOH 85%; LiCl 97-50%; $Li_2SO_4$ of 98% and 85%) with $Co(OH)_2$ as well as $CoSO_4$ as Co sources. The ECD of LCO was implemented in a cell comprised of a stainless-steel fiber current collector with 3D scaffold, Ni foil, and Co wire as working, counter, and quasi-reference electrodes, respectively, via applying potential pulses at 1.2 V. The 2 mAh $cm^{-2}$ loaded electrodes electrodeposited using the pulse ECD, delivered a specific capacity of around 145 mAh $g^{-1}$. The authors concluded that the electrodeposited LCO was not adversely affected by the low-purity precursors since they were capable of showing crystallinity and electrochemical performance as identical as the obtained LCO with pure precursors. The reported cyclic voltammogram (CV) profiles displayed the oxidation of $Co^{2+}$ at 0.6 V *vs.* $Co/Co^{2+}$ pseudo-reference electrode, regardless of the purity of the starting precursors, which confirms the robustness of ECD of LTMO.

Cook et al.[88] reported the commercialisation of the latter molten salt ECD to produce LCO films with a thickness of 500 µm on Al foil as microbattery electrodes without suffering from any trade-offs, such as lower power. This is due to the oriented monolithic morphology and textured structure of the electrodeposited LCO films with a preferred orientation of (110), which is acquired by tuning the ECD conditions, in contrast with the conventional slurry-casted films suffering from grain boundaries and fractures. The electrodeposited monolithic LCO film showed one order of magnitude higher $Li^+$ solid-state diffusion with a deliverable areal capacity of 9-12 mAh $cm^{-2}$.[88] They have also reported the ECD of electrodes with dimensions of 6 cm × 20 cm using a batch pilot plant (Fig. 3f). Further, they fabricated a microbattery with a multilayer stack of bipolar electrodes (Fig. 3g). The fabricated LIMB renders a specific capacity of ~ 160 mAh $g^{-1}$ at a rate of 0.1 C with an output voltage of ~ 4.0 V. Thus this method facilitates the fabrication of the different arrangements of a multi-layer stack with bipolar electrodes that causes the increased energy density by 10-15% as a consequence of the elimination of ~10 µm/electrode stack leads to high energy microbattery fabrication that would yield high energy of 600 Wh $kg^{-1}$ (1600 Wh $l^{-1}$).[88]

Following this direction, Pikul et al.[89] used a similar strategy to Zhang et al.[76] to develop an almost packaging-free primary LIMB possessing 50-80 mg and 20-40 µL of volume with the capability of delivering an energy density of 430 Wh $kg^{-1}$. They reported the ECD of 94% dense additive-free monolithic LCO with a thickness of up to 130 µm having an areal capacity of 12 mAh $cm^{-2}$. The higher thickness of the electrodeposited LCO did not penalize the rate capability as well as $Li^+$ diffusion kinetics due to the unique electrode architecture and controlled crystallographic orientation. The electrodeposited LCO possesses the preferred orientation with (110) parallel to the Al foil current collector (higher (110)/(113) and (110)/(003) peak ratios than LCO particles) which facilitated faster $Li^+$ diffusion compared to the conventional powder LCO with a mixture of orientations. The primary LIMB with the configuration of anode less/or pre-charged Li metal anodes (Figs. 3h and 3i) were able to deliver energy densities 4 times higher than previously reported analogues with the same size.

Braun et al.[90] also described molten salt ECD of air-sensitive O3-$Na_xMO_2$ (M = Co, Mn, Ni, Fe) in a molten hydroxide bath at 350 °C. This group reported ECD of $Na_xMnO_2$ and $Na_xCoO_2$ polycrystalline forms with a thickness of 10 µm (>75% dense) under 1 h. The electrodeposited phases were employed as binder/additive-free films as a cathode of sodium-ion batteries and delivered approximately the theoretical gravimetric capacities. Although sodium-ion batteries are out of the scope of the current review, we mention this work to highlight the generality of molten hydroxide salt ECD of both Li and Na transition metal oxides. On the other hand, the ECD of LTMOs such as $LiFeO_2$ has not been reported yet. Therefore, these works could pave the way for the ECD of these potentially cheaper LTMOs as the cathodes of LIMBs. However, the required temperature for this molten salt ECD of LTMOs (~350 °C) exceeds the thermal stabilities of the microelectronic components of LIMBs, thus requiring further optimizations to be compatible with microfabrication processes.

To conclude, ECD in molten salt opens a new path for synthesizing highly crystalline LTMOs at relatively lower temperatures compared to the conventional solid-state reaction methods. In addition, ECD enables the conformal as well as monolithic growth of active materials directly on the current collector and provides the opportunity to tune the desired electrode structures, from microstructure to flexibility, without making trade-offs between the energy and power density of the devices. However, most of the molten salt ECD of LTMOs reported so far mostly focused on LCO, and there is yet a long way to further develop this procedure for different Li-containing cathode materials such as $LiNi_xCo_yMn_zO_2$ (NMC) as well as $LiCo_xNi_yAl_yO_2$ (NCA) ideally at temperatures lower than 250 °C. Moreover, further research and development would be necessary to fully integrate the procedure of

direct ECD of various Li-containing cathode materials into the microfabrication protocols of LIMBs, as there are currently a few reports in this area. Finally, further research is essential to assess the thin-film ECD of the cathode materials on 3D nanostructures using this method to fabricate LIMBs. The research progress in the ECD of LCO on CNF and carbon foam scaffolds is insightful in this direction, but this needs to be further elaborated for the fabrication of 3D LIMBs.

**ECD of Li-containing cathode materials in ionic liquids**

Among the variously reported polyanions, LFP, with an ordered olivine structure, has been the only commercialized cathode material, owing to its high practical capacity of 170 mAh $g^{-1}$, flat voltage plateau (~ 3.4 V *vs*. $Li/Li^+$), and better thermal stability in its fully charged state, compared to LTMOs. LFP is therefore a highly attractive cathode material for LIMBs.[43,91] Additionally, LFP, due to its environmental friendliness and non-toxicity, is particularly beneficial for energy storage in medical implants.[92] Pulsed layer deposition (PLD),[92] radio frequency sputtering (RF sputtering),[93] electrostatic spray deposition (ESD),[94] and sol-gel methods[25] have been reported for the fabrication of LFP thin films. However, fabrication of LFP thin films using PLD and RF is an unlikely option for the microfabrication of LIMBs because they require (i) a high temperature of 600 °C and (ii) a post-annealing step at 600 °C to become fully electrochemically activated.[93,95,96] Despite the potential of ECD to produce LFP thin films, there are very few publications have been reported in this direction.

To the best of our knowledge, the research conducted by Guery et al.[97] is the only work in this direction. They reported a one-step electrochemically assisted synthesis of LFP(either as powder or film on Pt grid) using anhydrous $FeCl_3$ and $Li_3PO_4$ (in the ratio 2:1) in an ionic liquid 1-ethyl-3-methyl-imidazolium bis (trifluoromethanesulfonyl imide) [EMIm]TFSI. Using a Pt wire or disk as the working electrode, Ag wire as the reference electrode and Pt foil as the counter electrode (Fig. 4a-inset (i)), LFP was potentiostatically electrodeposited at – 0.3 V *vs* Ag and 275 °C. The results showed that the ECD for 5 hours led to an approximately pure phase of LFP with orthorhombic space group (Pnma) as confirmed by XRD patterns for the film LFP on Pt grid (Fig. 4a) and powder LFP (Fig. 4b). The electrodeposited LFP also exhibited the characteristic electrochemical behavior similar to the one obtained with conventional chemical synthesis methods reported in the previous literature (i.e. charge and discharge peaks at 3.5 and 3.4 V in the dQ/dV curve[98] (Fig. 4c). They elaborated the ECD pathway of LFP in the two steps: (1) electrochemical production of Fe (II) from Fe (III) precursor on the surface of working electrode, and (2) the subsequent chemical reaction of Fe (II) and insoluble $Li_3PO_4$.

However, the high viscosity and high cost of [EMIm]TFSI ionic liquid may require a different class of ionic liquid to enable the ECD of LFP. Nevertheless, this work paves the way for developing a one-step ECD of pure LFP films at lower temperatures with improved adherence and adaptability to the microfabrication strategies of LIMBs.

## ECD of Li-containing cathode materials in an aqueous medium

As discussed above, ECD in non-aqueous electrolytes is capable of producing conformal films of cathode materials with good electrochemical performance. However, there is still a need to develop ECD techniques in aqueous solutions under milder conditions that are compatible with microfabrication processes. Numerous researches have been dedicated to the direct ECD of LTMO films in aqueous media including lithium cobalt oxide (LCO), lithium nickel oxide (LNO), lithium vanadates (LVO), and lithium manganese oxides (LMO).

**$LiCoO_2$/$LiNiO_2$**

Several studies have been reported regarding the hydrothermal-assisted electrochemical syntheses (ECD-hydrothermal) of LTMO.[99–101] This so-called "soft solution processing (SSP)" method[102] can produce LTMO films with targeted crystallinity and composition. Yoshimura et al.[100] reported a single-step deposition of $Li_{1-x}Ni_{1+x}O_2$ on Ni substrate using an ECD-hydrothermal method in a concentrated LiOH aqueous solution at 150 °C (without any post-synthesis annealing). The ECD was done in an autoclave with a 3-electrode cell by applying a constant current density of 1 mA $cm^{-2}$ for 20 h. The electrodeposited $Li_{1-x}Ni_{1+x}O_2$ belongs to the R3m space group and showed crystalline grains with an average size of 0.23 µm. The cyclic voltammograms of the electrodeposited $Li_{1-x}Ni_{1+x}O_2$ at a scan rate of 5 mV $s^{-1}$ showed reversible redox behavior in 1.0 M $LiClO_4$/propylene carbonate solution, having oxidation and reduction peaks at ~ 4 V and ~ 3.3 V *vs.* $Li/Li^+$, respectively. [100] Also, the diffusion coefficient of the electrodeposited $Li_{1-x}Ni_{1+x}O_2$ was calculated to be $10^{-11}$ $cm^2$ $s^{-1}$, which was comparable to the previously reported values of $10^{-14}$ – $10^{-10}$ $cm^2$ $s^{-1}$ for LCO and LMO films prepared by other deposition techniques.[99,103,104] However, the peaks in the reported CV were not in total agreement with the redox peaks of the electrochemically active LNO.[105] A mechanism was suggested by Yoshimura et al.[99] for the possible reaction pathways to form $Li_{1-x}Ni_{1+x}O_2$ on the surface of the Ni substrate. This mechanism can be summarized in the following steps: (i) anodic dissolution of Ni and subsequent precipitation of $Ni(OH)_2$, (ii) formation of NiOOH and/or $NiOOH_{1-x}$•$H_2O$ film as a result of the second anodic step, (iii) cationic exchange of $H^+$ with $Li^+$ and dehydration. To support these, Han et al.[101] inferred the formation of various intermediates on the working electrode based on the potential evolution during ECD including $Ni(OH)_2$, NiOOH, $NiOOH_{1-x}$•$H_2O$, and described the following mechanism (Equations 2-5)**:**

$$Ni + 3\ OH^- \leftrightarrow HNiO_2^- + H_2O + 2e^- \quad \text{(Oxidative dissolution)} \quad (2)$$

$$HNiO_2^- + H_2O \rightarrow Ni(OH)_2 + OH^- \quad \text{(Precipitation)} \quad (3)$$

$Ni(OH)_2 + OH^- \rightarrow NiOOH + H_2O$ (Oxidation) (4)

$NiOOH + Li^+ + OH^- \rightarrow LiNiO_2 + H_2O$ (Cation exchange) (5)

However, the electrodeposited $Li_{1-x}Ni_{1+x}O_2$ film was not homogeneous in all the depth profiles. As the additional studies of the depth profile by XPS disclosed a compositional gradient of the film by proving the existence of $Ni(OH)_2$ and/or a NiOOH layer beneath the outer layers of electrodeposited $Li_{1-x}Ni_{1+x}O_2$.[106] Yoshimura et al.[106] showed that the prepared LNO films displayed reversible redox behavior with an oxidation peak at ~ 4.0 V and reduction peak at 3.3 V *vs*. $Li/Li^+$ in 0.1 M $LiClO_4$/propylene carbonate. Despite their similarity, the redox peaks were not consistent with the reported peaks for powder LNO electrodes in the literature.[105,107] Perhaps, this difference could be correlated with several phases of Li-Ni-O formed in the various depths of the film.

Tao et al.[108,109] used a similar ECD-hydrothermal technique, which was previously reported by Yoshimura et al.[100] to fabricate single-phase hexagonal LCO films on Co and Ni substrates. They used an electrolyte containing dissolved $Co(OH)_2$ in a 5 M LiOH aqueous solution at a constant temperature of 100 °C for 20 h. The electrodeposited LCO films exhibit a well-defined hexagonal lattice of α-$NaFeO_2$-R3m type with (003) and (101) oriented grains on Co and Ni substrates, respectively. This indicates that the type of substrate dramatically affects the crystallographical as well as morphological properties of the final electrodeposited LCO in terms of the preferred orientation of the planes. The deposited LCO film tended to grow in the vertical direction on the Co substrate leading to the preferred orientation of the (003) planes, as confirmed by the XRD. Further, the LCO crystals electrodeposited on polished nickel plates show a compact form while porous LCO crystals are formed and scattered on the surface of the nickel foam. This indicates that different formation mechanisms are involved in the film growth processes such as two-dimensional and preferential nucleation processes on polished nickel plates and nickel foams, respectively, depending on the nature of substrates. Moreover, the morphology, grain size, and porosity of the electrodeposited LCO crystals are influenced by the electrolyte concentration, current density, and temperature.[100] These electrodeposited LCO films on Co and Ni substrates exhibited reversible redox behavior having well-defined oxidation and reduction peaks at ~ 3.8 and 3.6 V *vs*. $Li/Li^+$ in 1 M $LiFP_6$/EC-DMC, indicating good electrochemical activity.[108]

Han et al.[110] used the same ECD-hydrothermal method as reported by Yoshimura et al.[100] for the direct deposition of LCO on the platinum or stainless steel substrates. This single-step ECD was performed by applying a constant current density of 2 mA $cm^{-2}$ with a fixed temperature within the range of 100 – 200 °C for 24 h without any post-synthesis steps. Here, Co metal powder was used as a cobalt source, which was located at the bottom of a stainless-steel autoclave. In addition to the electrodeposited film on the cathode, bulk LCO was also formed as a precipitate. The proposed reaction pathway based on the experimental data for the ECD of LCO was described below in Equations (6-8):

$Co + 3OH^- \rightarrow HCoO_2^- + H_2O + 2e^-$ Oxidative dissolution (6)

$HCoO_2^- + OH^- \rightarrow CoO_2^- + H_2O + e^-$ Presence of excess OH- at high temperature (7)

$CoO_2^- + Li^+ \rightarrow LiCoO_2$ Precipitation (8)

In this work,[110] authors have demonstrated that the excessive supply of hydroxyl groups influenced the morphology of the electrodeposited LCO. Here they galvanostatically generated the $OH^-$ groups by the electrolysis of water ($2H_2O + 2e^- \rightarrow 2OH^- + H_2$) at the surface of the cathode, which led to the further pH modification in conjunction with the high concentration of the alkaline solution. The morphological investigations on the electrodeposited LCO films showed layered structures with observable boundaries between layers on the substrate. This was an implication of the lower density of the electrodeposited film than the theoretical density of LCO (5.06 $g.cm^{-3}$). The electrodeposited LCO formed by the direct ECD technique displays high-purity crystallinity and belongs to the R3m space group with a Li/Co ratio of 1, which is comparable to the LCO prepared via solid-state technique at 800-1000 °C. However, these electrodeposited LCO films with a thickness of 1.3 μm exhibited an initial discharge capacity of only half (51.4%) of the theoretical discharge capacity of LCO. It also showed poor cycling stability, retaining only 23% of the initial discharge capacity after 100 cycles. To improve the electrochemical performance of electrodeposited LCO, strenuous efforts have to be taken to optimize the extrinsic parameters of the film such as density, integrity, contact, and adhesion between cathode film and the substrate.[110]

Following these developments, many works have been conducted to adopt these ECD procedures to fabricate electrodes for high-performance LIMB either by adjusting substrates or direct patterning by skipping the post-annealing steps. Yoshimura et al.[111] reported a one-step ECD of LCO film using a flow-cell reactor enabling the direct patterning of the film. Using this method, they were able to control the pattern of electrodeposited LCO by merely altering the configuration of the carbon rod anode (columnar or chisel-like). To obtain LCO film on the substrate (either on the filter paper or on the hydrophilic polytetrafluoroethylene (PTFE) membrane filter mounted on the carbon rod anode), a constant current density was applied at 120 °C in an electro-furnace between working and counter electrodes in an aqueous solution of LiOH and 0.1 M $CoSO_4.7H_2O$. According to the suggested mechanism, $CoO_2^-$ is initially formed as a result of $Co^{2+}$ oxidation, then the succeeding reaction takes place depending on the $Co^{2+}$ concentration in the electrolyte i.e. high concentration of $Co^{2+}$ leads to the transformation of $CoO^{2-}$ to $Co_3O_4$, whereas low $Co^{2+}$ concentration leads to the formation of the desired LCO.[111] However, the reported XRD pattern of the electrodeposited LCO was not well-matched with the XRD pattern of layered R3m LCO synthesized via conventional methods at 800 − 1000 °C. Therefore, major optimizations of the electrode material/configuration have to be conducted before considering this strategy as an efficient method for direct patterning.

Chen et al[112] utilized the anodic ECD-hydrothermal technique to regenerate LCO thin film in a solution extracted from the cathode of spent Li-ion batteries through leaching by nitric acid. They used a two-electrode system in a highly concentrated solution of LiOH under a constant temperature of 100 °C in a sealed PTFE autoclave. The deposited LCO thin film on the Ni plate delivered an initial discharge capacity of 127.1 mAh $g^{-1}$ and retained almost 97% of the initial discharge capacity after 30 cycles at 0.1 C.[112] However, despite the fairly good electrochemical performance, the reported XRD patterns of the electrodeposited LCO were not well-matched with the electroactive layered phase of LCO with the R3m space group. Nevertheless, this research propounded the tremendous potential of ECD for recycling precious metals such as Co, and Li from spent LIB, which could replace the current recycling strategies that have plenty of drawbacks in terms of safety, energy consumption, multi-step procedures, and environmental concerns.

To avoid the adverse effects of high pressure on the deposited film, Han et al.[113] reported the synthesis of layered LCO film via galvanostatic electrochemical reflux method under the ambient pressure without using any autoclave. They reported the deposition of a well-crystallized pure phase of LCO films with an R3m space group, having a thickness of ~ 12 μm. The ECD was done in a mixture of 1 M LiOH and 12 M KOH solution as the electrolyte and the presence of Co powder at the fixed temperatures within the range of 100-200 °C. The obtained layered LCO film exhibited an initial discharge capacity of 54.1 μA $cm^{-2}$ $\mu m^{-1}$ which was retained up to 85.6% upon 15 cycles. These results demonstrated the potential of aqueous ECD at ambient pressure to electrodeposit well-crystallized R3m electroactive LCO films. Considering the adherence as well as the integrity of the produced LCO films, these ECD procedures could be facilely adjusted to the LIMB fabrication procedures. However, the reported electrochemical performance in comparison with the obtained results from molten salt ECD of LCO was far from expected values for high-performance LIMBs.

Lai et al.[114] described the ECD of LCO at room temperature on Co substrate. They also investigated the influence of different experimental conditions on the crystalline structure and morphology of the electrodeposited LCO films. They found that the crystallinity, densification, and uniformity of the electrodeposited LCO films increased with the electrochemical reaction time, current density as well as the concentration of the LiOH solution. At room temperature under optimal conditions (current density of 1 mA $cm^{-2}$, 3 M LiOH, and treatment time of 50 h), the synthesized LCO films, with a thickness of 5 μm on the cobalt substrate, exhibits a single-phase hexagonal layered structure. Nonetheless, the electrodeposited LCO under optimized ECD conditions could not be considered a well-crystallized R3m phase. The electrochemical performance of the electrodeposited LCO films exhibits a potential plateau at ~ 3.9 V *vs.* $Li/Li^+$ in 1.0 M $LiPF_6$/EC/DEC, designating the typical properties for the layered LCO phase. Even though this group did not examine the comprehensive electrochemical performance of the electrodeposited LCO, the reported primary data is promising enough to pursue the research in this area with highly interesting ECD conditions at room temperature and ambient pressure, which has to be incorporated into the fabrication procedure of LIMB.

Porthault and coworkers[115] electrodeposited LCO films on various substrates (titanium foil, protected silicon wafer substrate, etc.) via the one-step electrochemical-hydrothermal method, without any further post-treatment procedures. They utilized an electrolyte containing $Co(NO_3)_2$•$6H_2O$ dissolved in an aqueous solution of LiOH, and the ECD was performed in a galvanostatic mode at 150-200 °C for 1 h. At 150 °C, they obtained a highly dense homogeneous LCO film with a thickness of about 6.5 μm and 6.8 μm on the titanium and wafer substrates, respectively, indicating a significantly higher deposition rate of approximately 110 nm/min compared to the sputtering method (10 nm/min). Further, the XRD analysis revealed the crystalline nature of LCO with the R3m space group having different preferred orientations dependent on the substrate material. Also, the deposited LCO on the protected silicon wafer had a regular columnar growth pattern with a density of 4.54 g $cm^{-3}$ which is good considering the theoretical value of LCO is 5.06 g $cm^{-3}$. Moreover, the theoretical study of the potential–pH diagram for cobalt species showed that an increase in the temperature and a decrease in the cobalt concentration could stabilize the soluble species (assumed to be involved in the LCO formation) at high pH. The cyclic voltammetric measurements of the electrodeposited LCO films in the potential window of 4.2–3.0 V exhibited a reversible redox behavior with characteristic peaks of the layered R3m hexagonal LCO. The prepared LCO thin film at 200 °C showed better electrochemical performance in terms of cyclability, retaining 90% of the first discharge capacity after 50 cycles at C/5. However, increasing the temperature beyond 200 °C resulted in the formation of an impurity phase of $Co_3O_4$.

In their next attempt, Porthault et al.[116] investigated the effect of an electrolyte by employing an ethanol-water blend electrolyte to electrodeposit LCO thin films on titanium foil substrate through the ECD-hydrothermal method. They investigated the influence of different synthesis parameters such as ethanol/water ratio, current density temperature, pressure, and reaction time on the crystalline structure, morphology, and electrochemical behavior of the electrodeposited LCO films. They observed that adding ethanol as cosolvent enables the use of higher current densities and hence increases the deposition rate up to 500 nm $min^{-1}$, leading to smoother surface morphology.

Moreover, long deposition time (1 h to 4 h) has been found to increase the porous nature of the film surface and consequently decrease the density of the film. Further, the electrodeposited LCO films treated under a higher temperature of 400 °C show enhanced electrochemical behavior, with an initial capacity of 60 μAh $cm^{-2}$. $\mu m^{-1}$ when cycled between 3.0 and 4.2 V *vs.* $Li/Li^+$ at a C/5 rate, which is 87% of the theoretical volumetric discharge capacity with capacity fading of 0.1%/cycle for 130 cycles, for the film treated at 400 °C. However, this post-annealing step makes this procedure highly unfavorable as it not only deteriorates the adherence of the film to the substrate but also restricts the incorporation of this ECD step into the fabrication of LIMB.

The same group has also reported the preparation of LCO thin film on the surface of 3D metalized textured silicon substrates by using the ECD-hydrothermal method as shown in the SEM image (Fig. 5a).[117] Additionally, they fabricated self-standing 3D LCO electrodes on platinum instead of titanium substrates, so that the electrode layers can be easily stripped off from the patterned surface due to the poor adhesion between the platinum and the electrodeposited LCO films. They followed the same procedure of thin-film preparation as reported in the previous research at 125 °C.[115] The electrodeposited thin film consisted of $Li_{0.92}CoO_2$ with a well-crystallized R3m structure and as dense as 90% of the theoretical density of LCO. The capacity of electrodeposited LCO thin film on the surface of square and rectangular pyramids patterned silicon wafers is almost equal to the capacity of the electrodeposited thin film on the flat substrate (35 μAh $cm^{-2}$ $\mu m^{-1}$ preserving 80% of the initial capacity after 50 cycles and 75% after 100 cycles at 30 μA $cm^{-2}$) (Fig. 5b). Further, they have fabricated a full cell battery device with the

electrodeposited LCO films (both planar and 3D films) by depositing LiPON solid-state electrolytes and Ti layers using PVD techniques. This work demonstrated the capability of the ECD method to fabricate 3D LIMB either by using a 3D textured substrate or by depositing 3D self-standing LCO thin films (Fig. 5c). The results of this research on LCO in aqueous medium could be considered more promising compared to the hitherto reported results in the literature, since they were able to produce the conformal dense films of LCO either on the flat or textured substrates via ECD at relatively low temperature and high deposition rate, which delivers good electrochemical performance. Though crystalline structure of the electrodeposited LCO was not perfectly matching with R3m space group, this research still could be highly inspiring for more research and development on the ECD in aqueous medium under milder conditions to be successfully incorporated to the microfabrication techniques of LIMBs.

Apart from the ECD-hydrothermal method which uses the anodic ECD approach to electrodeposit the films, there are a few approaches employing cathodic ECD. For instance, Yen et al.[118] reported the deposition of $LiCo_2O_4$ coating on stainless steel type 304 substrate by taking the advantage of cathodic ECD from a mixture of $LiNO_3$ and $Co(NO_3)_2.6H_2O$ by applying a constant potential of -0.9 V *vs.* Ag/AgCl (saturated KCl) and then subsequent transformation to $LiCo_2O_4$ under thermal annealing at 310 °C, which was further transformed to LCO and $Co_3O_4$ mixture when annealed at 500 °C. The obtained $LiCo_2O_4$ film showed a discharge plateau around 3.5 V *vs.* $Li/Li^+$ as well as a reversible capacity of 70 mAh $g^{-1}$ at 10 μA $cm^{-2}$ within the range of 3.8 and 3.2 V *vs.* $Li/Li^+$, which is corresponding to 50% of the theoretical capacity, and also maintains a discharge capacity of 67.5 mAh $g^{-1}$ even after 50 cycles. However, the formed LCO was not stable for $Li^+$ insertion/extraction due to the presence of $Co_3O_4$ by product.[118] Again, this reported procedure for the production of LCO/$LiCo_2O_4$ films is not very favourable as it entails a post-annealing step which could damage the integrity and adhesion of the film to the substrate and, more importantly, impedes the adoption of this procedure to LIMB fabrication procedures. But it sheds light on the new perspectives to explore and develop one-step cathodic ECD of LCO or the other LTMOs with pure crystalline phase as well as better electrochemical performance.

So far, we have discussed the ECD of LCO, LNO, and $LiCo_2O_4$ cathode materials mainly by using the hydrothermal-assisted ECD along with a few works reporting ECD at room temperature/atmosphere pressure technique. We analyzed various factors such as electrolyte compositions, current densities, temperature, etc., that influence the crystallinity, morphology, and microstructural properties of the electrodeposited films. Though the layered R3m phase with electrochemical activity could be accomplished via applying this ECD technique, the electrochemical performance is inferior compared to that of the molten salt ECD technique. Thus, it seems unlikely that this technique could compete with the molten salt ECD approach, at least at this current stage of its development. Further research and development in this area are required to develop aqueous-media ECD under milder conditions (ideally at room temperature/atmospheric pressure) to deposit conformal films of pure crystalline phases of LCO/LNO, $LiNi_xCo_yO_2$ (LNCO) with the comparable electrochemical performance of the conventionally obtained or molten salt electrodeposited counterparts.

**ECD of LVOs**

LVOs, with high discharge capacity and suitable charge/discharge plateaus corresponding to transitions between its various oxidation states ($V^{2+}$, $V^{3+}$, $V^{4+}$ and $V^{5+}$), have emerged as promising cathode materials of LIB.[119–121] There are a few studies that have described the ECD of LVO thick films and employed it as the cathode of LIBs. For example, Watanabe et al.[122] explored an ECD-hydrothermal method to derive βII-$Li_3VO_4$ orthorhombic single phase on a vanadium plate substrate. This ECD procedure was done in a 4 M LiOH aqueous solution in an autoclave at hydrothermal conditions of 150 °C without any post-annealing. They used autogenerated pressure of 15 MPa for 24 h via applying a current density of 1 mA.$cm^{-2}$. According to the reported XRD pattern, the lattice parameters of the prepared material without any post-annealing were identical to those previously reported at high temperature-mediated solid-state synthesized orthorhombic βII-$Li_3VO_4$. [122] This group did not provide any electrochemical activity of the prepared $Li_3VO_4$ thin films.

In another attempt, Fang et al.[123] fabricated $Li_{0.04}V_2O_5$ nanowires through ECD via potentiostatic method for 7 h at 90 °C on a Ti foil substrate in a bath containing mixtures of $NH_4VO_3$, oxalic acid, hexamethylene tetramine, and $LiNO_3$. The as-prepared $Li_{0.04}V_2O_5$ thick films, possessing high tap density, comprised of intertwined nanowires with a thickness of ~11.1 μm (Fig. 5d). However, the electrodeposited $Li_{0,04}V_2O_5$ showed low crystalline nature, which was converted to the orthorhombic crystalline phase of $Li_{0.04}V_2O_5$ (PDF card No: 85-0608) after annealing at 200-400 °C. The electrodeposited $Li_{0.04}V_2O_5$, after annealing at 200 °C, delivered a discharge capacity of 228.78 mAh $g^{-1}$ at a current density of 50 mA $g^{-1}$, which reduced to 123.7 mAh $g^{-1}$ after 100 cycles. (Figs. 5e and 5f). Moreover, they have also investigated the influence of applied potential, temperature, and time on the thickness of the electrodeposited nanowire arrays.[123] However, the electrodeposited $V_2O_5$ was far from fully lithiated phases, which would restrict the application of that in full cell LIMB.

**ECD of lithium manganese oxides**

Mn-based cathode materials, owing to the abundance of Mn, their non-toxicity, environmental benignity, and high discharge capacity, are considered among the most attractive options as thin-film cathode materials for LIB and LIMB.[124] However, thin-film fabrication of LMOs requires high-temperature processes, either during post-annealing procedures (350 - 700 °C)[125] or high-temperature deposition processes such as PLD (700 - 800 °C).[126,127] These high temperatures may be detrimental to microelectronic components of LIMB. Therefore, developing one-step ECD of $LiMnO_2$/LMO conformal thin films at a lower temperature at a fast deposition speed (higher than magnetron sputtering technique, where deposition of a thin film of orthorhombic $LiMnO_2$ with a thickness of 1.4 μm takes ~ 4 hrs [128]) is a challenge yet to be addressed. In this regard, numerous researches have been trying to establish single-step ECD of thin films of $Li_xMnO_2$ by taking the advantage of amorphous[129] as well as diverse tunnel structures of $MnO_2$[83] such as γ[77,130] and birnessite layered δ-$MnO_2$.[27]

In this regard, Popov et al.[131] used one-step potentiostatic ECD employing a 3-electrode cell for 60 min in an aqueous bath containing $MnSO_4$ and chlorate salts of alkali cations. They reported ECD of a layered type $MnO_2$ on the Au-sputtered stainless steel, the so-called birnessite phase, which was intercalated with alkali metal cations including $Li^+$, $Na^+$, and $Mg^{2+}$ and exploited as the cathode material for Li-ion battery. The alkali metals cation incorporation happened as a result of the electrostatic interactions between negatively charged layers of birnessite phase of $MnO_2$ and the alkali metal cations according to the following reaction (Equation 9):

$$Mn^{2+} + (2+n)\ H_2O + xA^{c+} \rightarrow \underset{c}{A_x}Mn_x^{3+}Mn_{1-x}^{4+}O_2.nH_2O + 4\ H_2O + 4\ H^+ + (2-x)\ e^- \quad (\boldsymbol{n \approx 1}) \qquad (9)$$

Where A is the alkali cation, and c is 1 for $Li^+$ and $Na^+$ or 2 for $Mg^{2+}$. The amount of intercalated cations was correlated to the composition of the ECD bath and applied potential. The electrodeposited $Li_{0.35}MnO_2.H_2O$ delivered an initial gravimetric discharge capacity of 73 mAh $g^{-1}$ and also an areal capacity of 10 µAh $cm^{-2}$ (Fig. 6a) while applying a discharge current density of 10 µA $cm^{-2}$ followed by decaying to 56 mAh $g^{-1}$ after 8 cycles (Fig. 6b).[131,132] Also, morphology investigations showed uniform coverage of the $Li_{0.35}MnO_2.H_2O$ film with a rugged surface on the substrate (Fig. 6c). They have also suggested the possibility of further stabilizing the layered structure with an R3m lattice symmetry by substituting Mn elements with Co and Ni, which could be inspiring for future research on the one-step fabrication of cathode materials in the film format.

Nakayama et al.[133] performed another research on the cathodic ECD of alkaline cations containing birnessite-type $MnO_2$ in 2 mM $KMnO_4$ aqueous solution containing 50 mM of different alkaline metal cations including $Li^+$. This procedure was done at a constant potential of 0 V *vs.* Ag/AgCl (saturated KCl) on polycrystalline Pt foil in a 3-electrode standard ECD cell. The deposition mechanism was expressed as the following reaction Equation 10:[133,134]

$$MnO_4^- + 2\ H_2O + (3+x)e^- + xA^+ \rightarrow A_xMn_x^{3+}Mn_{1-x}^{4+} + 4\ OH^- \qquad (10)$$

Even though only the capacitive performance of the obtained $Li_xMnO_2$ birnessite phases was probed, supposedly based on the previously reported results by Nakayama et al.,[131] this electrodeposited $Li_xMnO_2$ is prone to undergoing (de)lithiation as cathode material of LIB/LIMB. Additionally, the cathodic ECD used in this work could be advantageous, as the applied cathodic potential would not oxidize metallic substrates, which could enable the use of a broader range of substrates. However, to the best of our knowledge, despite its potential for forming conformal films of $Li_xMnO_2$ on various substrates, there are no reports on the cathodic ECD of $Li_xMnO_2$ for use as a cathode of LIB/LIMBs.

Javanbakhtet et al.[135–138] performed an anodic galvanostatic ECD of $Li_xMnO_2$ on stainless steel as a working electrode to investigate the impact of applying continuous,[135] pulse[136] and pulse reverse[137,138] current regimes on the physicochemical and electrochemical properties of final electrodeposited $Li_xMnO_2$. They proved that the crystalline phase, the amount of inserted lithium ions, and subsequently the electrochemical performance of electrodeposited $Li_xMnO_2$ could be manipulated with the regime of the applied current. They reported one-step galvanostatic ECD of mesoporous $Li_xMnO_2$ (x = 0.07 – 0.33), predominantly comprised of γ phases along with traces of α crystalline phase. The results show that the amount of $Li^+$ inserted into the host structure of $MnO_2$ was modified by changing the composition of the ECD bath.[135] Further studies[136–138] by this group also demonstrated the influence of ECD via pulse and pulse reverse current on the $Li^+$ content (within the range of 0.19 −0.65), morphology as well as surface area, which ultimately affects the electrochemical performance of $Li_xMnO_2$ as a cathode material for LIB (Figs. 6d-6i).[136,137] It has been found that the application of optimum values of pulse with a duty cycle of 0.1 and pulse reverse current parameters with a duty cycle of 0.79, increased the amount of $Li^+$ inserted in the electrodeposited $Li_xMnO_2$ ( x= 0.4 for pulse and x = 0.65 for pulse reverse current). The electrodeposited $Li_{0.41}MnO_2$ under optimized pulse current with a duty cycle of 0.1 produced entangled nano-flake structures (Fig. 6d) capable of delivering a first discharge capacity of 284 mAh $g^{-1}$, retaining ~94% of it after 250 cycles at 0.1 C (Figs. 6e and 6f). Furthermore, applying the optimized pulse reverse current with a duty cycle of 0.79 led to a hierarchical urchin-like nano/microstructure of $Li_xMnO_2$ (Fig. 6g), having a BET surface area of ~320 $m^2\ g^{-1}$ with mixed γ/α crystal. The obtained $Li_{0.65}MnO_2$ was able to deliver a first discharge capacity of ~283 mAh $g^{-1}$ and retain 88.3% of this capacity after 300 cycles at 0.1 C[137] (Figs. 6h and 6i).

It should be mentioned that the electrodeposited $Li_xMnO_2$ by this group was not electrochemically examined as a thin film in LIB and the scratched deposited material was slurry cast on Al foil after mixing and grinding with graphite and polyvinylidene fluoride (PVDF). Moreover, the electrodeposited $Li_xMnO_2$ was subjected to a post-annealing step at 375 °C to remove crystalline water. Therefore, this research could not be directly regarded as a feasible procedure to be integrated into the microfabrication protocols of LIMBs. Nonetheless, this work could enlighten the path to achieving desirable $LiMnO_2$ thin films in terms of physicochemical and electrochemical properties by controlling the deposition method.

Although numerous research has dealt with the ECD of $MnO_2$ thin films as cathode for LIB/LIMB, to the best of the authors' knowledge, there is no reported research on the one-step ECD of $Li_xMnO_2$ thin films with a Li/Mn ratio of 1. Moreover, there is also no report on the direct single-step ECD of LMO with Fd3m spinel crystal structure. Rather, most of the works have focused on the ECD of $Mn_3O_4$ thin films, followed by an annealing step at a high temperature in the range of 700 -1000 °C, which is not suitable for LIMBs.[139] In summary, most research has mainly focused on the one-step ECD of lithiated γ- and δ-$MnO_2$ from aqueous media; however, fabrication of fully lithiated $MnO_2$ through one-step ECD procedures yet remains a challenge. Undoubtedly, considering the advantages of $LiMnO_2$/LMO as thin-film cathodes for LIMB, intensive research and development are required to develop strategies adaptable to the microfabrication conditions of LIMBs.

All the discussed ECD techniques in the various electrolytes have been summarized based on the cathode material, ECD medium, applied ECD technique, and the electrochemical performance of the electrodeposited cathode material in Table 1. Additionally, Table 2 summarizes the advantages and disadvantages of various applied ECD methods based on ECD medium. Overall, by comparing the electrochemical performance of electrodeposited Li-containing cathode materials either in LIBs or LIMBs (Table 1), it has been found that the electrodeposited conformal cathodic films through the molten salt medium exhibits better performance in terms of discharge capacity and cyclic stability even at higher C-rates in half-cell as well as full cell LIMB/LIB configurations without any post-annealing procedures.

Most likely, the preferential orientation of monolithic electrodeposited LCO with (110) planes parallel to the current collector could be considered as the most interesting aspect of molten salt ECD. Because this textured electrodeposited LCO with (110) could enables the fastest $Li^+$ diffusion pathways leading to high gravimetric capacity without penalizing the power density even at the higher thickness ($1 - 500$ μm) and is highly promising to attain LIMBs with high power and high energy density. On the other hand, the electrochemical performance of the electrodeposited films of cathode materials (mainly LCO) in aqueous medium is not good enough to be integrated to the microfabrication procedure of high performance LIMBs. However, the aqueous electrodeposited cathodic material reported by Porthault et al.[117] is promising for the microfabrication techniques and also inspiring to pursue the research in this direction with the merits of mild temperature and fast deposition in a shorter span of time. Additionally, the hitherto reported electrodeposited LMOs and LVOs did not exhibit good electrochemical performance and the $Li^+$ deficiency in the chemical composition would hamper their application in the full cell configurations.

## ECD of Li-free cathode materials

Previous sections have exclusively focused on the one-step ECD of Li-containing cathode materials, which would be ideal for full-cell LIMB fabrication in the discharged state. In addition, the materials with little to no Li-content are also found to be feasible cathode material, which is now a day attaining more interest in Li-metal based batteries and microbatteries.[85]. As previously discussed, development of Li metal batteries, thanks to the progression of solid-state electrolyte as well as metallic lithium (anode),[140] could trigger the opportunity of using Li-free cathode materials. The Li-free cathode materials such as $MnO_2$, $FeS_2$ etc., which were dominantly being used in the first decade of lithium battery development era, experiencing a reincarceration as pointed out by Li et al..[85,141] The use of Li-free cathode materials, mainly transition metal sulfides ($FeS_2$) and transition metal oxides (such as $MnO_2$[77,130] $V_2O_5$[28], and $MoO_3$[142]), in lithium metal batteries enables high gravimetric energy density (high specific capacity as well as high operating voltage) and can be assembled in charged state leading to higher safety levels.[143,144] The ECD technique of these Li-free cathode materials is well-established and could be facilely realized as conformal thin films on 3D substrates. Therefore along with the possibility of Li metal anode deposition, the ECD of Li-free cathode materials can be used to fabricate lithium matal based microbatteries with high energy density.[28,130] Nonetheless, regardless of the outstanding advantages of low cost, environmental friendliness and abundance, this category of cathode materials could practically benefit microbatteries only after tackling the challenges related to voltage hysteresis, volume change, capacity fade, parasitic reactions and poor electronic and ionic conductivity in the case of metal oxides. Li et al.[85] have categorized and discussed the main strategies to addressing these challenges. Here, in Table 3, we have summarized the ECD of different and well-known Li-free cathode materials to fabricate conformal thin films for lithium metal based batteries and microbatteries by covering the details related to the ECD conditions and electrochemical performance.

## Perspectives and Outlook

A transition from 2D to 3D configuration in LIMBs is essential to make a leap in energy and power densities to meet the essential requirements of LIMBs as the promising power sources of microelectronics. One of the main bottlenecks for designing 3D LIMBs is the conformal coating of thin-film cathode materials on 3D substrates under mild conditions, which has hindered the development of high-power LIMBs. Among the various technologies available, ECD is a robust technique to realize 3D thin-film electrodes by precisely controlling the parameters and also follows mild conditions, which is more compatible with the fabrication of 3D LIMBs. It is noteworthy that several disadvantages such as the lack of controlling the quality of the electrodeposited film in the atomic scale, the poor adherence, precise controlling of the chemical composition of the electrodeposit as well as the entailment of using conductive substrate could hinder the widespread use of ECD as film fabrication technique. Also, ECD is not suitable for the fabrication of epitaxial films as compared to ALD technique. Nevertheless, ECD could be considered as a powerful technique to accomplish the conformal films of the targeted electroactive materials by subtle selection of the ECD technique, chemical composition of the electrolyte as well as the substrate. Also, by ECD technique it could be possible to obtain high quality films of Li-containing cathode materials as thoroughly discussed in this paper.

In this work, we have reviewed most of the published research on one-step ECD of Li-containing cathode materials for LIB/LIMBs, including lithium transition metal oxides, $LiMO_2$ (M = Ni, Co, Mn), spinel LMO, LVOs and olivine (LFP) materials in aqueous and non-aqueous (molten salt and ionic liquid) media. From the literature survey, it is found that molten hydroxide salt is the best non-aqueous electrolyte for one-step ECD of different Li-containing cathode materials such as conformal LCO, spinel LMO, and Al-doped LCO films on a variety of substrates. The structural and electrochemical properties of these electrodeposited materials, formed at a comparatively low temperature of 260 °C, exhibit identical features to those materials obtained from solid-state synthesis at 700-1000 °C. This clearly illustrates the potential of one-step molten-salt ECD which can be integrated into the 3D LIMB fabrication. Moreover, the commercialization of this molten slat ECD of LTMO (high purity monolithic films of LCO) as cathode for high-energy LIMBs,[88] shows more promising towards the large scale implementation of this technology. Therefore, this approach could be a suitable option to be optimized to fabricate conformal thin films of different LTMO cathode materials including various compositions of high voltage NMC ($LiCo_xNi_yMn_yO_2$, x+y+z = 1), $LiNi_xCo_yAl_zO_2$ (NCA) and spinel phase of $LiNi_{0.5}Mn_{1.5}O_4$, by controlling the composition of the eutectic molten salt in the ECD bath. Although, the reported temperature of the molten salt ECD is relatively compatible with the processes and constituents of LIMBs fabrication, this temperature might be crossing the tolerable region while considering the full integration of microfabrication procedures with susceptible integrated circuits and flexible plastic parts. Therefore, developing the molten salt ECD method at a lower temperature without penalizing its efficiency would be essential to fully take advantage of this procedure for LIMB fabrication procedures. The use of ionic liquids would provide the ECD of LTMO thin films at a much lower temperature than that in molten salt. However, unlike the molten salt method, using a non-aqueous medium of ionic liquids has not been extensively investigated and, seemingly, LFP is the only cathode material that has been electrodeposited in ionic liquids. This study is of great importance, as it demonstrates the feasibility of one-step ECD of LFP film and powder without post-annealing. Efficient ECD techniques for LFP conformal films could be developed by optimizing this method.

Single-step ECD of $LiMO_2$ (M = Co, Ni, Mn), LVO and spinel $LiCo_2O_4$, whether via electrochemical or electrochemical-hydrothermal methods have been extensively discussed in the aqueous bath. Among the reported research on ECD of Li-containing cathode materials in an aqueous bath, LCO seems to be the most feasibly electrodeposited, forming pure R3m layered crystal structure even when electrodeposited at room temperature and ambient pressure. Despite a great deal of progress made in this direction, the performance of materials electrodeposited from aqueous media is still inferior to those electrodeposited from molten salt electrolytes. The drawbacks of materials electrodeposited by single-step ECD from aqueous solutions are (1) difficulty with obtaining the fully lithiated phase in one step, leading to Li-deficient phases with limited performance in full cell LIMBs; (2) inferior adhesion and conformality of the obtained film; (3) low density and integrity of the electrodeposited film; and (4) difficulty in attaining the desired crystalline structure and electrochemical performance without any post-annealing treatments. Circumventing these challenges requires intense research to develop an optimized composition of ECD bath as well as finding appropriate ECD techniques. Moreover, to date, there are no published studies on the aqueous ECD of lithium mixed transition metal oxides such as $LiNi_xMn_yCo_zO_2$ (NMC) and $LiNi_xCo_yAl_zO_2$ (NCA) as thin-film cathode materials. However, the research done by Inoue et al.[145] to electrodeposit Li-V-Mn-Ni-O composite films directly on Al foils could open new avenues for further development of the ECD of this class cathode materials. In short, more research on the ECD of LTMO thin films in an aqueous solution is essential, since this method is comparatively cost-effective and can be implemented in ambient conditions.

Besides Li-containing cathode materials, conformal thin film deposition of Li-free cathode materials (including $MnO_2$, $V_2O_5$, $MoO_xS_y$, and $FeS_2$) via ECD has been well established and holds a big potential to benefit all the solid-state lithium metal based microbatteries with the high energy density. However, some of the reported ECD techniques of Li-free cathode materials employ a post-annealing step within the range of 300-400 °C specifically in the case of electrodeposited $MnO_2$, which is not favorable. And necessarily this post-annealing step needs to be removed or at least to be implemented at lower temperatures to be compatible with the fabrication strategies of microbatteries.

It is noteworthy that ECD of Li-containing Prussian blue analogous (PBA) in the form of thin films[82] could open new paths to accomplish high-energy LIMBs under highly moderate conditions of ECD. Also, ECD of Na-containing Prussian blue analogues thin films with very positive $Na^+$ (de)intercalation potentials in aqueous Na-ion batteries (such as $Na_2VO_x[Fe(CN)_6]$[146] and $Na_2Ni[Fe(CN)_6]$[147]) might likely create a new paradigm in aqueous Na-ion batteries, which could be promising and might be extended to the lithiated films to be employed as a cathode of LIMBs. Moreover, co-deposition of already-prepared cathode materials with conducting polymers[148–150] or pure metals (such as Ag or Au[151]) could be explored for thin-film preparation of other cathode materials such as NMC and $LiNi_{0.5}Mn_{1.5}O_4$ as a simple and adaptable alternative technique instead of vapor-phase techniques such as PLD or magnetron sputtering.

Finally, although ECD is yet to be extensively used to synthesize thin or thick films of LIMBs as a result of the above-mentioned challenges, developing ECD systems in molten salt, organic, ionic liquid, as well as aqueous media under compatible conditions with microfabrication, would be of advantage to developing cheap, high-energy and high power LIMBs.

## Conflicts of interest

The authors declare no conflict of interest.

## Acknowledgments

The authors acknowledge the CF-ARC grant (18/23-093) MICROBAT for financial support.

## References

[1] W. Lee, S. Muhammad, C. Sergey, H. Lee, J. Yoon, Y.M. Kang, and W.S. Yoon, *Angew. Chemie - Int. Ed.* **59**, 2578 (2020).
[2] A. Manthiram, *Nat. Commun.* **11**, 1 (2020).
[3] S. Moitzheim, B. Put, and P.M. Vereecken, *Adv. Mater. Interfaces* **6**, 1 (2019).
[4] B. Babu, P. Simon, and A. Balducci, *Adv. Energy Mater.* **10**, 2001128 (2020).
[5] Q. Liu, G. Zhang, N. Chen, X. Feng, C. Wang, J. Wang, X. Jin, and L. Qu, *Adv. Funct. Mater.* **2002086**, 1 (2020).
[6] M. Nasreldin, R. Delattre, C. Calmes, M. Ramuz, V.A. Sugiawati, S. Maria, J.-L. de B. de la Tocnaye, and T. Djenizian, *Energy Storage Mater.* **33**, 108 (2020).
[7] K. Edström, D. Brandell, T. Gustafsson, and L. Nyholm, *Electrochem. Soc. Interface* **20**, 41 (2011).
[8] M.J. Synodis, M. Kim, M.G. Allen, and S.A.B. Allen, *J. Micromechanics Microengineering* **29**, 055006 (2019).
[9] J. Shi, S. Liu, L. Zhang, B. Yang, L. Shu, Y. Yang, M. Ren, Y. Wang, J. Chen, W. Chen, Y. Chai, and X. Tao, *Adv. Mater.* **32**, 1 (2020).
[10] X. Wang, Y.L. Ding, Y.P. Deng, and Z. Chen, *Adv. Energy Mater.* **10**, 1 (2020).
[11] N.A. Kyeremateng and R. Hahn, *ACS Energy Lett.* **3**, 1172 (2018).
[12] M. Zhu and O.G. Schmidt, *Nature* **589**, 195 (2021).
[13] L. Liu, Q. Weng, X. Lu, X. Sun, L. Zhang, and O.G. Schmidt, *Small* **13**, 1 (2017).
[14] Z. Zhu, R. Kan, S. Hu, L. He, X. Hong, H. Tang, and W. Luo, *Small* **16**, 1 (2020).
[15] Y. Wu, X. Huang, L. Huang, and J. Chen, *ENERGY Environ. Mater.* **4**, 19 (2021).
[16] S. Zheng, X. Shi, P. Das, Z.S. Wu, and X. Bao, *Adv. Mater.* **31**, 1 (2019).
[17] Y. Horowitz, E. Strauss, E. Peled, and D. Golodnitsky, *Isr. J. Chem.* 1 (2021).
[18] S. Ferrari, M. Loveridge, S.D. Beattie, M. Jahn, R.J. Dashwood, and R. Bhagat, *J. Power Sources* **286**, 25 (2015).
[19] J. Ni, A. Dai, Y. Yuan, L. Li, and J. Lu, *Matter* **2**, 1366 (2020).
[20] J.W. Long, B. Dunn, D.R. Rolison, and H.S. White, *Adv. Energy Mater.* **10**, (2020).
[21] J.W. Long, B. Dunn, D.R. Rolison, and H.S. White, *Chem. Rev.* **104**, 4463 (2004).
[22] V. Zadin, H. Kasemägi, A. Aabloo, and D. Brandell, *J. Power Sources* **195**, 6218 (2010).
[23] N. Labyedh, F. Mattelaer, C. Detavernier, and P.M. Vereecken, *J. Mater. Chem. A* **7**, 18996 (2019).
[24] X. Wang, X. Fan, X. Yu, S. Bak, Z. Shadike, I. Waluyo, A. Hunt, S.D. Senanayake, H. Li, L. Chen, C. Wang, R. Xiao, E. Hu, and X. Yang, *Adv. Funct. Mater.* **31**, 2001633 (2021).
[25] J. Mosa, M. Aparicio, A. Durán, C. Laberty-Robert, and C. Sanchez, *J. Mater. Chem. A* **2**, 3038 (2014).
[26] H. Xia, Y. Wan, W. Assenmacher, W. Mader, G. Yuan, and L. Lu, *NPG Asia Mater.* **6**, e126 (2014).
[27] Q. Xia, Q. Zhang, S. Sun, F. Hussain, C. Zhang, X. Zhu, F. Meng, K. Liu, H. Geng, J. Xu, F. Zan, P. Wang, L. Gu, and H. Xia, *Adv. Mater.* **33**, 1 (2021).
[28] P. Sun, X. Li, J. Shao, and P. V. Braun, *Adv. Mater.* **33**, e2006229 (2021).
[29] F. Mattelaer, K. Geryl, G. Rampelberg, J. Dendooven, and C. Detavernier, *ACS Appl. Mater. Interfaces* **9**, 13121 (2017).
[30] T. Dobbelaere, F. Mattelaer, J. Dendooven, P. Vereecken, and C. Detavernier, *Chem. Mater.* **28**, 3435 (2016).

[31] M. Nathan, D. Golodnitsky, V. Yufit, E. Strauss, T. Ripenbein, I. Shechtman, S. Menkin, and E. Peled, *J. Microelectromechanical Syst.* **14**, 879 (2005).
[32] H. Mazor, D. Golodnitsky, L. Burstein, and E. Peled, *Electrochem. Solid-State Lett.* **12**, 232 (2009).
[33] D. Golodnitsky, V. Yufit, M. Nathan, I. Shechtman, T. Ripenbein, E. Strauss, S. Menkin, and E. Peled, *J. Power Sources* **153**, 281 (2006).
[34] S.R. Gowda, A. Leela Mohana Reddy, X. Zhan, H.R. Jafry, and P.M. Ajayan, *Nano Lett.* **12**, 1198 (2012).
[35] H.S. Min, B.Y. Park, L. Taherabadi, C. Wang, Y. Yeh, R. Zaouk, M.J. Madou, and B. Dunn, *J. Power Sources* **178**, 795 (2008).
[36] K. Sun, T.S. Wei, B.Y. Ahn, J.Y. Seo, S.J. Dillon, and J.A. Lewis, *Adv. Mater.* **25**, 4539 (2013).
[37] D. Cao, Y. Xing, K. Tantratian, X. Wang, Y. Ma, A. Mukhopadhyay, Z. Cheng, Q. Zhang, Y. Jiao, L. Chen, and H. Zhu, *Adv. Mater.* **31**, 1807313 (2019).
[38] H. Ning, J.H. Pikul, R. Zhang, X. Li, S. Xu, J. Wang, J.A. Rogers, W.P. King, and P. V. Braun, *Proc. Natl. Acad. Sci. U. S. A.* **112**, 6573 (2015).
[39] J.H. Pikul, H. Gang Zhang, J. Cho, P. V. Braun, and W.P. King, *Nat. Commun.* **4**, 1 (2013).
[40] H. Zhang, X. Yu, and P. V. Braun, *Nat. Nanotechnol.* **6**, 277 (2011).
[41] C. Liu, E.I. Gillette, X. Chen, A.J. Pearse, A.C. Kozen, M.A. Schroeder, K.E. Gregorczyk, S.B. Lee, and G.W. Rubloff, *Nat. Nanotechnol.* **9**, 1031 (2014).
[42] J. Graetz, C.C. Ahn, R. Yazami, and B. Fultz, *J. Electrochem. Soc.* **151**, A698 (2004).
[43] X.J. Zhu, L. Bin Cheng, C.G. Wang, Z.P. Guo, P. Zhang, G.D. Du, and H.K. Liu, *J. Phys. Chem. C* **113**, 14518 (2009).
[44] J.F.M. Oudenhoven, T. van Dongen, R.A.H. Niessen, M.H.J.M. de Croon, and P.H.L. Notten, *J. Electrochem. Soc.* **156**, D169 (2009).
[45] Y. Matsuda, N. Kuwata, and J. Kawamura, *Solid State Ionics* **320**, 38 (2018).
[46] J.F.M. Oudenhoven, L. Baggetto, and P.H.L. Notten, *Adv. Energy Mater.* **1**, 10 (2011).
[47] O. Nilsen, V. Miikkulainen, K.B. Gandrud, E. Østreng, and A. Ruud, *Phys. Status Solidi Appl. Mater. Sci.* **211**, 357 (2014).
[48] M. Maximov, D. Nazarov, A. Rumyantsev, Y. Koshtyal, I. Ezhov, I. Mitrofanov, A. Kim, O. Medvedev, and A. Popovich, *Energies* **13**, 2345 (2020).
[49] Y. Yang, W. Yuan, X. Zhang, Y. Yuan, C. Wang, Y. Ye, Y. Huang, Z. Qiu, and Y. Tang, *Appl. Energy* **257**, 114002 (2020).
[50] Z. Lyu, G.J.H. Lim, J.J. Koh, Y. Li, Y. Ma, J. Ding, J. Wang, Z. Hu, J. Wang, W. Chen, and Y. Chen, *Joule* **5**, 89 (2021).
[51] D.S. Kolchanov, I. Mitrofanov, A. Kim, Y. Koshtyal, A. Rumyantsev, E. Sergeeva, A. Vinogradov, A. Popovich, and M.Y. Maximov, *Energy Technol.* **8**, 1 (2020).
[52] P. Yang and H.J. Fan, *Adv. Mater. Technol.* **5**, 1 (2020).
[53] Y. Lee, *Energies* **12**, 658 (2019).
[54] Y. Kang, C. Deng, Y. Chen, X. Liu, Z. Liang, T. Li, Q. Hu, and Y. Zhao, *Nanoscale Res. Lett.* **15**, 112 (2020).
[55] K. Fu, Y. Wang, C. Yan, Y. Yao, Y. Chen, J. Dai, S. Lacey, Y. Wang, J. Wan, T. Li, Z. Wang, Y. Xu, and L. Hu, *Adv. Mater.* **28**, 2587 (2016).
[56] J. Li, M.C. Leu, R. Panat, and J. Park, *Mater. Des.* **119**, 417 (2017).
[57] J. Huang, J. Yang, W. Li, W. Cai, and Z. Jiang, *Thin Solid Films* **516**, 3314 (2008).
[58] C. Lethien, M. Zegaoui, P. Roussel, P. Tilmant, N. Rolland, and P.A. Rolland, *Microelectron. Eng.* **88**, 3172 (2011).
[59] J. Pu, Z. Shen, C. Zhong, Q. Zhou, J. Liu, J. Zhu, and H. Zhang, *Adv. Mater.* **32**, 1 (2020).
[60] Z. Qi and H. Wang, *Research* **2020**, 1 (2020).
[61] L. Benea, P.L. Bonora, A. Borello, S. Martelli, F. Wenger, P. Ponthiaux, and J. Galland, *J. Electrochem. Soc.* **148**, C461 (2001).
[62] I. Gurrappa and L. Binder, *Sci. Technol. Adv. Mater.* **9**, 043001 (2008).
[63] T. Yoshida, J. Zhang, D. Komatsu, S. Sawatani, H. Minoura, T. Pauporté, D. Lincot, T. Oekermann, D. Schlettwein, H. Tada, D. Wöhrle, K. Funabiki, M. Matsui, H. Miura, and H. Yanagi, *Adv. Funct. Mater.* **19**, 17 (2009).
[64] Y. Yuan and A. Lei, *Nat. Commun.* **11**, 2018 (2020).
[65] L. Lu and H. Nagai, *Lithium-Ion Batteries - Thin Film for Energy Materials and Devices* p.17, IntechOpen London (2020).
[66] K. Zhang, Z. Yan, and J. Chen, *Joule* **4**, 10 (2020).
[67] M. Synodis, J. Pikul, S. Ann Bidstrup Allen, and M.G. Allen, *J. Power Sources* **449**, 227566 (2020).
[68] Y. Lu, Z. Tu, and L.A. Archer, *Nat. Mater.* **13**, 961 (2014).
[69] J. Zheng, Q. Zhao, T. Tang, J. Yin, C.D. Quilty, G.D. Renderos, X. Liu, Y. Deng, L. Wang, D.C. Bock, C. Jaye, D. Zhang, E.S. Takeuchi, K.J. Takeuchi, A.C. Marschilok, and L.A. Archer, *Science* **366**, 645 (2019).
[70] Z. Li, Y. Zhou, Y. Wang, and Y.C. Lu, *Adv. Energy Mater.* **9**, 1 (2019).
[71] A. Lahiri and F. Endres, *J. Electrochem. Soc.* **164**, D597 (2017).
[72] J.O. Omale, R. Rupp, P. Van Velthem, V. Van Kerckhoven, V.-A. Antohe, A. Vlad, and L. Piraux, *Energy Storage Mater.*

**21**, 77 (2019).
[73] A.C. Johnson, R. Kohlmeyer, M.N. Ates, C. Kiggins, A. Blake, X. Yue, J.B. Cook, and J.H. Pikul, p.1, *19th Int. Conf. Micro Nanotechnol. Power Gener. Energy Convers. Appl.* Poland (2019).
[74] M.M. Shaijumon, E. Perre, B. Daffos, P.L. Taberna, J.M. Tarascon, and P. Simon, *Adv. Mater.* **22**, 4978 (2010).
[75] G. Oltean, L. Nyholm, and K. Edström, *Electrochim. Acta* **56**, 3203 (2011).
[76] H. Zhang, H. Ning, J. Busbee, Z. Shen, C. Kiggins, Y. Hua, J. Eaves, J. Davis, T. Shi, Y.-T.T. Shao, J.-M.M. Zuo, X. Hong, Y. Chan, S. Wang, P. Wang, P. Sun, S. Xu, J. Liu, and P. V. Braun, *Sci. Adv.* **3**, 1 (2017).
[77] P. Johns, M. Roberts, and J. Owen, *J. Mater. Chem.* **21**, 10153 (2011).
[78] G.D. Salian, C. Lebouin, A. Demoulin, M.S. Lepihin, S. Maria, A.K. Galeyeva, A.P. Kurbatov, and T. Djenizian, *J. Power Sources* **340**, 242 (2017).
[79] S.G. Patnaik, A. Jadon, C.C.H. Tran, A. Estève, D. Guay, and D. Pech, *Sci. Rep.* **10**, 1 (2020).
[80] X. He, Y. Yang, M.S. Cristian, J. Wang, X. Hou, B. Yan, J. Li, T. Zhang, E. Paillard, M. Swietoslawski, R. Kostecki, M. Winter, and J. Li, *Nano Energy* **67**, 104172 (2020).
[81] G.R. Li, H. Xu, X.F. Lu, J.X. Feng, Y.X. Tong, and C.Y. Su, *Nanoscale* **5**, 4056 (2013).
[82] S.G. Patnaik and D. Pech, *Small* **17**, 1 (2021).
[83] M.Y. Timmermans, N. Labyedh, F. Mattelaer, S.P. Zankowski, S. Deheryan, C. Detavernier, and P.M. Vereecken, *J. Electrochem. Soc.* **164**, 954 (2017).
[84] E. Armstrong, D. McNulty, H. Geaney, and C. ODwyer, *ACS Appl. Mater. Interfaces* **7**, 27006 (2015).
[85] L. Wang, Z. Wu, J. Zou, P. Gao, X. Niu, H. Li, and L. Chen, *Joule* **3**, 2086 (2019).
[86] W.K. Ham, G.F. Holland, and A.M. Stacy, *J. Am. Chem. Soc.* **110**, 5214 (1988).
[87] M.N. Ates, J.D. Busbee, C.T. Kiggins, and J.B. Cook, US20190363340A1 (2019).
[88] J.B. Cook, R. Kohlmeyer, C. Kiggins, M.N. Ates, A. Blake, J.D. Busbee, P. Braun, S. Kim, A. Johnson, X. Yue, and J.H. Pikul, in *GOMAC Tech, San Diego* (2020).
[89] X. Yue, A.C. Johnson, S. Kim, R.R. Kohlmeyer, A. Patra, J. Grzyb, A. Padmanabha, M. Wang, Z. Jiang, P. Sun, C.T. Kiggins, M.N. Ates, S. V. Singh, E.M. Beale, M. Daroux, A.J. Blake, J.B. Cook, P. V. Braun, and J.H. Pikul, *Adv. Mater.* **33**, 1 (2021).
[90] A. Patra, J. Davis, S. Pidaparthy, M.H. Karigerasi, B. Zahiri, A.A. Kulkarni, M.A. Caple, D.P. Shoemaker, J.M. Zuo, and P. V. Braun, *Proc. Natl. Acad. Sci.* **118**, e2025044118 (2021).
[91] A. Manthiram and J.B. Goodenough, *Nat. Energy* **6**, 844 (2021).
[92] Z.G. Lu, M.F. Lo, and C.Y. Chung, *J. Phys. Chem. C* **112**, 7069 (2008).
[93] K.-F. Chiu, H.-Y. Tang, and B.-S. Lin, *J. Electrochem. Soc.* **154**, A364 (2007).
[94] J. Ma and Q.-Z. Qin, *J. Power Sources* **148**, 66 (2005).
[95] V.A. Sugiawati, F. Vacandio, C. Perrin-Pellegrino, A. Galeyeva, A.P. Kurbatov, and T. Djenizian, *Sci. Rep.* **9**, 1 (2019).
[96] K.-F. Chiu, *J. Electrochem. Soc.* **154**, A129 (2007).
[97] Y. Chen, J.M. Tarascon, and C. Guéry, *Electrochem. Commun.* **13**, 673 (2011).
[98] J. Shim and K.A. Striebel, *J. Power Sources* **119**–**121**, 955 (2003).
[99] K. Han, P. Krtil, and M. Yoshimura, *J. Mater. Chem.* **8**, 2043 (1998).
[100] K.S. Han, S.W. Song, and M. Yoshimura, *Chem. Mater.* **10**, 2183 (1998).
[101] M. Yoshimura, K.-S. Han, and S. Tsurimoto, *Solid State Ionics* **106**, 39 (1998).
[102] K.S. Han, S.W. Song, S. Tsurimoto, H. Fujita, I. Sasagawa, K.H. Choi, H.K. Kang, and M. Yoshimura, *Solid State Ionics* **151**, 11 (2002).
[103] K.A. Striebel, C.Z. Deng, S.J. Wen, and E.J. Cairns, *J. Electrochem. Soc.* **143**, 1821 (1996).
[104] P. Birke, W.F. Chu, and W. Weppner, *Solid State Ionics* **93**, 1 (1996).
[105] T. Deng, X. Fan, L. Cao, J. Chen, S. Hou, X. Ji, L. Chen, S. Li, X. Zhou, E. Hu, D. Su, X.-Q.Q. Yang, and C. Wang, *Joule* **3**, 2550 (2019).
[106] K. Han, S. Song, H. Fujita, and M. Yoshimura, *Solid State Ionics* **135**, 273 (2000).
[107] M. Broussely, F. Perton, J. Labat, R.J. Staniewicz, and A. Romero, *J. Power Sources* **43**, 209 (1993).
[108] Y. Tao, Z. Chen, B. Zhu, and W. Huang, *Solid State Ionics* **161**, 187 (2003).
[109] Y. Tao, B. Zhu, and Z. Chen, *J. Cryst. Growth* **293**, 382 (2006).
[110] K.-S. Han, S.-W. Song, H. Fujita, M. Yoshimura, E.J. Cairns, and S.-H. Chang, *J. Am. Ceram. Soc.* **85**, 2444 (2002).
[111] T. Fujiwara and M. Yoshimura, *J. Electroanal. Chem.* **559**, 63 (2003).
[112] L. Li, R. Chen, F. Sun, F. Wu, and J. Liu, *Hydrometallurgy* **108**, 220 (2011).
[113] J.H. Lee, K.S. Han, B.J. Lee, S. Il Seo, and M. Yoshimura, *Electrochim. Acta* **50**, 467 (2004).
[114] D. Gao, Y. Li, X. Lai, J. Bi, and D. Lin, *J. Alloys Compd.* **509**, 697 (2011).
[115] H. Porthault, F. Le Cras, R. Baddour-Hadjean, J.P. Pereira-Ramos, and S. Franger, *Electrochim. Acta* **56**, 7580 (2011).
[116] T. Azib, F. Le Cras, and H. Porthault, *Electrochim. Acta* **160**, 145 (2015).
[117] H. Porthault, F. Le Cras, J.M. Duffault, and S. Franger, *Mater. Sci. Eng. B Solid-State Mater. Adv. Technol.* **213**, 163 (2016).

[118] W.-Y. Shieh, T.-C. Chang, and S.-K. Yen, *J. Electrochem. Soc.* **160**, A1128 (2013).
[119] V. Pralong, V. Gopal, V. Caignaert, V. Duffort, and B. Raveau, *Chem. Mater.* **24**, 12 (2012).
[120] M. Qin, W. Liu, S. Liang, and A. Pan, *Trans. Nonferrous Met. Soc. China* **26**, 3232 (2016).
[121] Z. Chen, F. Xu, S. Cao, Z. Li, H. Yang, X. Ai, and Y. Cao, *Small* **13**, 1 (2017).
[122] T. Watanabe, W.S. Cho, W.L. Suchanek, M. Endo, Y. Ikuma, and M. Yoshimura, *Solid State Sci.* **3**, 183 (2001).
[123] K. Hua, X. Li, D. Fang, J. Yi, R. Bao, and Z. Luo, *Appl. Surf. Sci.* **447**, 610 (2018).
[124] P. Liu, J. Zhang, J.A. Turner, C.E. Tracy, and D.K. Benson, *J. Electrochem. Soc.* **146**, 2001 (1999).
[125] J. Fischer, C. Adelhelm, T. Bergfeldt, K. Chang, C. Ziebert, H. Leiste, M. Stüber, S. Ulrich, D. Music, B. Hallstedt, and H.J. Seifert, *Thin Solid Films* **528**, 217 (2013).
[126] H. Tan, K. Kamala Bharathi, I. Takeuchi, and L.A. Bendersky, *Thin Solid Films* **638**, 282 (2017).
[127] M. Fehse, R. Trócoli, E. Ventosa, E. Hernández, A. Sepúlveda, A. Morata, and A. Tarancón, *ACS Appl. Mater. Interfaces* **9**, 5295 (2017).
[128] J. Fischer, K. Chang, J. Ye, S. Ulrich, C. Ziebert, D. Music, B. Hallstedt, and H.J. Seifert, *Thin Solid Films* **549**, 263 (2013).
[129] L. Chen, A. van Zomeren, and J. Schooman, *Solid State Ionics* **67**, 203 (1994).
[130] Y. Zargouni, S. Deheryan, A. Radisic, K. Alouani, and P. Vereecken, *Nanomaterials* **7**, 126 (2017).
[131] M. Nakayama, T. Kanaya, J.-W.W. Lee, and B.N. Popov, *J. Power Sources* **179**, 361 (2008).
[132] M. Nakayama, T. Kanaya, J.-W. Lee, and B. Popov, *ECS Trans.* **11**, 35 (2008).
[133] M. Nakayama, M. Nishiyama, M. Shamoto, T. Tanimoto, K. Tomono, and R. Inoue, *J. Electrochem. Soc.* **159**, A1176 (2012).
[134] M. Shamoto, T. Tanimoto, K. Tomono, and M. Nakayama, *ECS Meet. Abstr.* **MA2012-02**, 544 (2012).
[135] S. Behboudi-Khiavi, M. Javanbakht, S.A.S.A. Mozaffari, and M. Ghaemi, *J. Electroanal. Chem.* **801**, 224 (2017).
[136] S. Behboudi-Khiavi, M. Javanbakht, S.A.S.A. Mozaffari, and M. Ghaemi, *Electrochim. Acta* **261**, 491 (2018).
[137] S. Behboudi-Khiavi, M. Javanbakht, S.A. Mozaffari, and M. Ghaemi, *ACS Appl. Mater. Interfaces* **11**, 21552 (2019).
[138] S. Behboudikhiavi, M. Javanbakht, S.A. Mozaffari, and M. Ghaemi, US 10,865,493 B2 (2020).
[139] Z. Quan, S. Ohguchi, M. Kawase, H. Tanimura, and N. Sonoyama, *J. Power Sources* **244**, 375 (2013).
[140] Y. Chen, J. Li, Z. Lei, Y. Huo, L. Yang, S. Zeng, H. Ding, Y. Qin, Y. Jie, F. Huang, Q. Li, J. Zhu, R. Cao, G. Zhang, S. Jiao, and D. Xu, *Adv. Energy Mater.* **10**, 1903401 (2020).
[141] L. Hongliang, W. Kaiyuan, Y. Zi, Z. Quanchao, and C. Yanhua, *Chem. Phys.* **544**, 111111 (2021).
[142] M.A. Spencer, O. Yildiz, I. Kamboj, P.D. Bradford, and V. Augustyn, *Energy and Fuels* **35**, 16183 (2021).
[143] I.K. Hewavitharana, Y. Ding, K.Y.Y. Simon Ng, and D. Deng, *Chem. Eng. Sci.* **236**, 116480 (2021).
[144] V.R. Punyapu, Y. Ding, K.Y. Simon Ng, and D. Deng, *Ind. Eng. Chem. Res.* **61**, 7474 (2022).
[145] T. Inoue, S.-Z.S. Kure-Chu, Y. Moriguchi, R. Miyazaki, T. Hihara, and H. Yashiro, *ECS Meet. Abstr.* **MA2019-01**, 355 (2019).
[146] B. Paulitsch, J. Yun, and A.S. Bandarenka, *ACS Appl. Mater. Interfaces* **9**, 8107 (2017).
[147] P. Marzak, J. Yun, A. Dorsel, A. Kriele, R. Gilles, O. Schneider, and A.S. Bandarenka, *J. Phys. Chem. C* **122**, 8760 (2018).
[148] Y.-H. Huang, K.-S. Park, and J.B. Goodenough, *J. Electrochem. Soc.* **153**, A2282 (2006).
[149] K.S. Park, S.B. Schougaard, and J.B. Goodenough, *Adv. Mater.* **19**, 848 (2007).
[150] Y.H. Huang and J.B. Goodenough, *Chem. Mater.* **20**, 7237 (2008).
[151] A. Eftekhari, *J. Electrochem. Soc.* **151**, A1816 (2004).
[152] Y. Zargouni, S. Deheryan, A. Radisic, D.J. Cott, S. Rochan, K. Alouani, C. Huyghebaert, and P.M. Vereecken, *ECS Trans.* **61**, 29 (2014).
[153] L.M. McGrath and J.F. Rohan, *Batter. Supercaps* **4**, 485 (2021).
[154] K. Freedman, V. Yufit, D. Golodnitsky, M. Nathan, and E. Peled, *ECS Meet. Abstr.* 2 (2007).
[155] V. Yufit, D. Golodnitsky, L. Burstein, M. Nathan, and E. Peled, *J. Solid State Electrochem.* **12**, 273 (2008).
[156] V. Yufit, K. Freedman, M. Nathan, L. Burstein, D. Golodnitsky, and E. Peled, *Electrochim. Acta* **50**, 417 (2004).

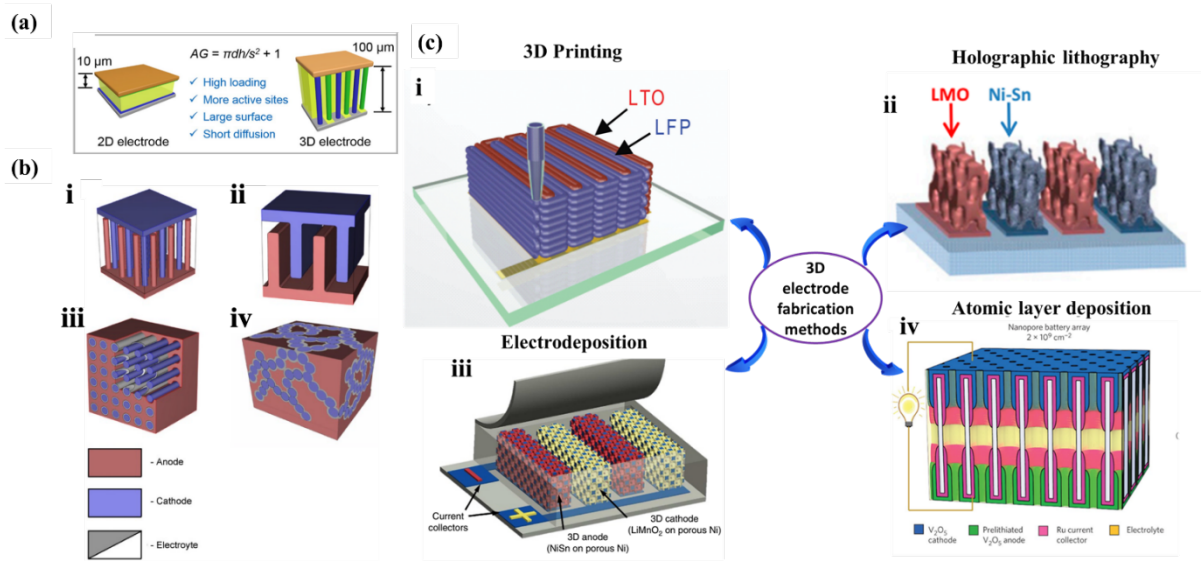


**Figure 1**. (a) Comparison of 2D to 3D LIMB configurations and benefits of 3D over 2D architectures; the inset formula describes the area gain, where *d* is the nanorod diameter, *s* is the nanorod spacing, and *h* nanorod height. Reproduced with permission from ref. [19]. Copyright 2020, Elsevier. (b) Possible architectures of 3D LIMBs, including: (i) interdigitated, (ii) trench, (iii) concentric, and (iv) aperiodic electrode designs. Reproduced with permission from ref.[22]. Copyright 2010, Elsevier. (c) Summary of the representative 3D electrode fabrication techniques: (i) Schematic illustration of interdigitated architectures made by 3D printing. Reproduced with permission from ref [36]. Copyright 2013, Wiley-VCH. (ii) Schematic illustration of the 3D microbatteries fabricated by a combination of 3D holographic and conventional lithography. Reproduced with permission from ref.[38]. Copyright 2015, Proceeding of the National Academy of Sciences of the United States of America. (iii) Microbattery constituents fabricated via electrodeposition on Ni scaffold using a colloidal template. Reproduced with permission from ref.[39]. Copyright 2013, Springer Nature. and (iv) Schematics of nanopore battery arrays and their cross-section made by step-wise deposition of battery constituents within alumina nanoporous templates with the ALD technique.; Reproduced with permission from ref.[41]. Copyright 2014, Springer Nature.

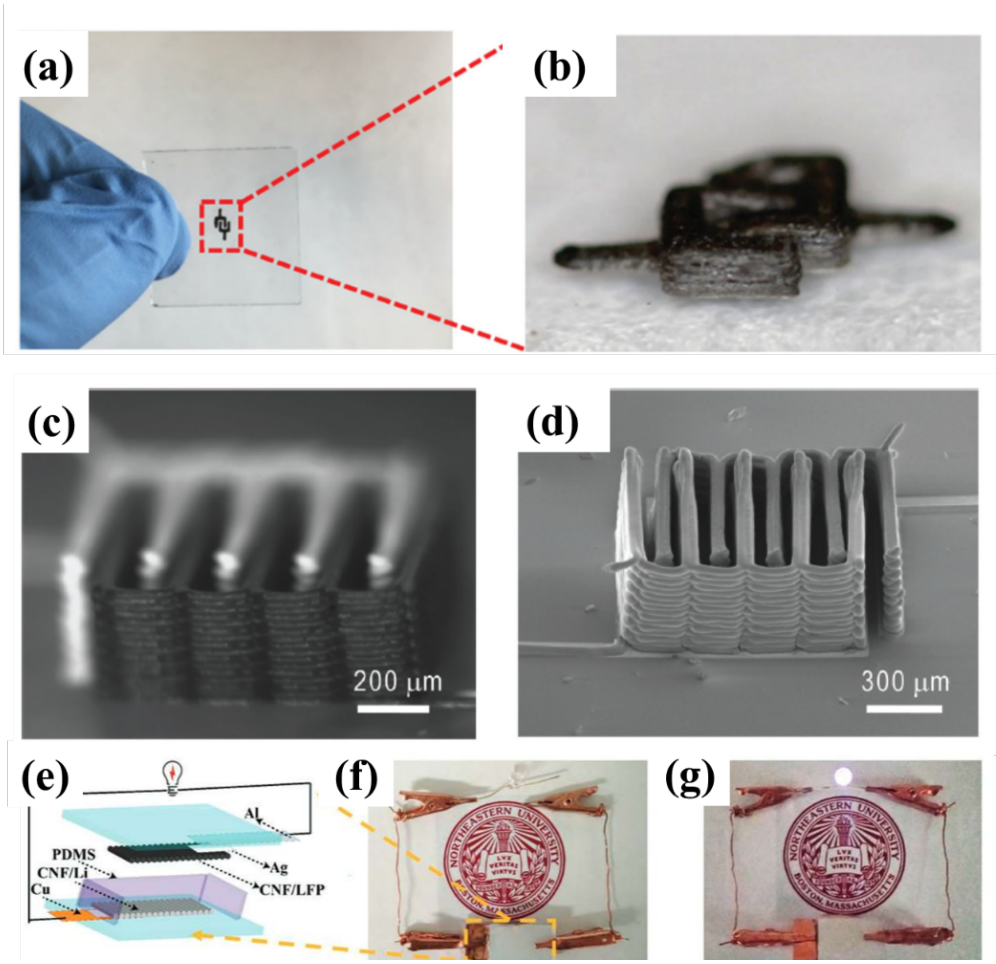


**Figure 2**. (a, b) Digital images of the miniaturized version of 3D printed electrodes on a glass substrate based on LFP/reduced graphene oxide (rGO) composite as the cathode and $LiTi_5O_{12}$ (LTO)/rGO as the anode. Reproduced with permission from ref [55]. Copyright 2016, Wiley-VCH. (c) Optical and (d) SEM images of printed LTO/LFP interdigit LIMB. Each electrode is print-stacked in 16-layers. Reproduced with permission from ref [36]. Copyright 2013, Wiley-VCH. (e) Schematic view of a cell with printed electrodes. Cellulose nanofibers (CNF)/Li and CNF/LFP were used as anode and cathode, respectively. Photographs of the packaged planar LIMB assembled by extrusion-based 3D-printed cathode and anode secured on Al and Cu foils respectively by Ag paste (f) before and (g) after connecting to a white LED lamp with an operating voltage higher than 3.0 V. Reproduced with permission from ref [37]. Copyright 2019, Wiley-VCH.

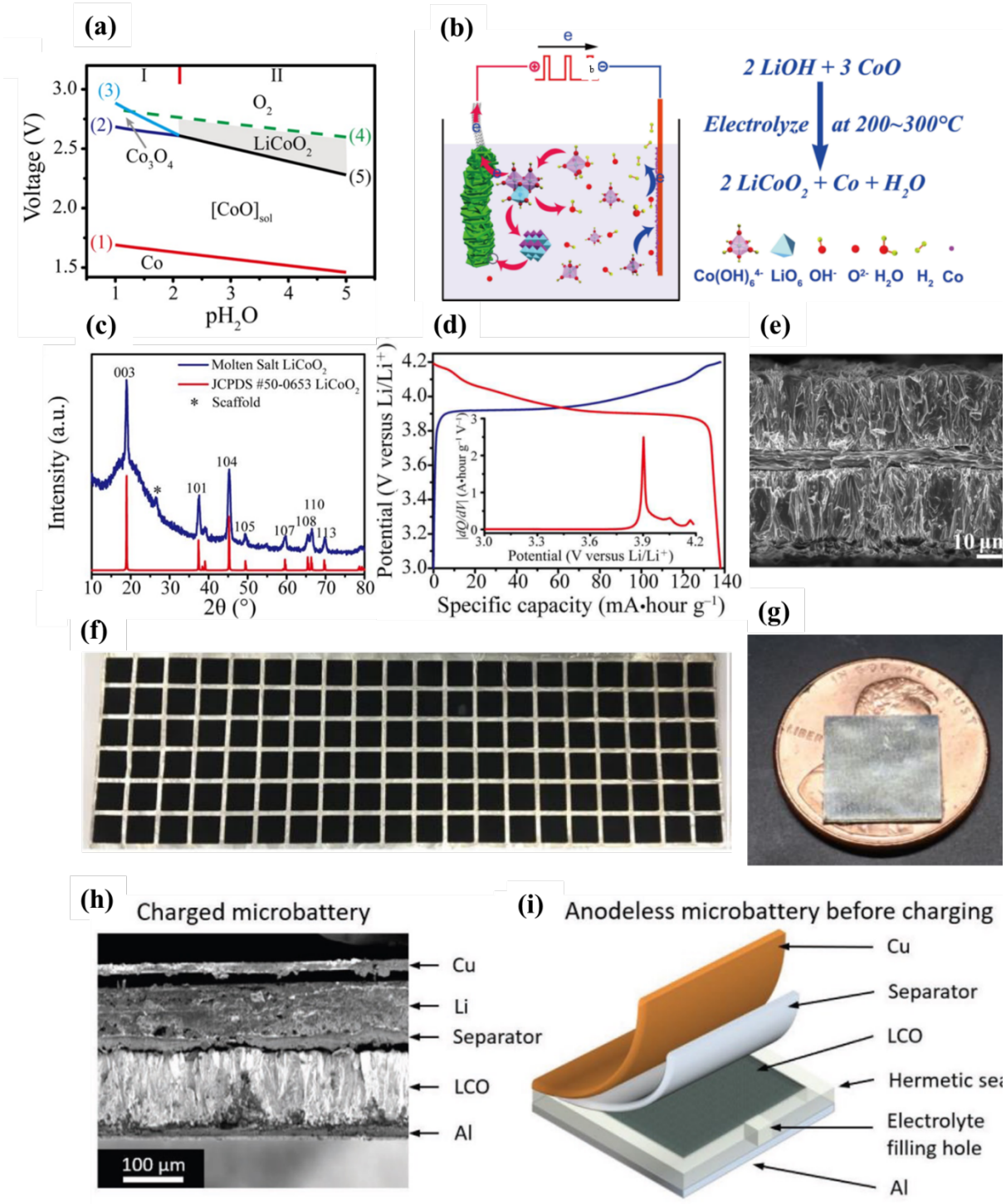


**Figure 3.** (a) Potential-$pH_2O$ diagram of LiOH-KOH-CoO eutectic system used for the ECD of LCO, (b) Schematic illustration of ECD process of LCO, (c) XRD pattern confirming the R3m phase of electrodeposited LCO, (d) corresponding charge-discharge profiles measured in Li half cells (inset: |dq/dV| of the electrodeposited LCO on an Al foil). (e) SEM image of electrodeposited planar LCO film (~20% porosity) electroplated on both sides of an Al foil. Reproduced with permission from ref [76]. Copyright 2017, Science. (f) Photograph of 6 cm x 20 cm array of microbattery electrodes made using Xerion Advanced Battery Corp. (g) Photograph of the microbattery electrodes utilizing the molten salt electrodeposited LCO as the cathode (The US 1¢ coin is used for scaling). Reproduced with permission from ref.[88].Copyright 2020, Proceeding GOMAC Tech, San Diego. (h) cross-section SEM image of charged microbattery comprising of electrodeposited LCO cathode and Li anode. (i) schematic illustration of anodeless microbattery before charging with four components including an LCO cathode electrodeposited on 23 µm Al foil, a bare 9-µm Cu foil (anodeless design). Reproduced with permission from ref [89]. Copyright 2021, Wiley-VCH .

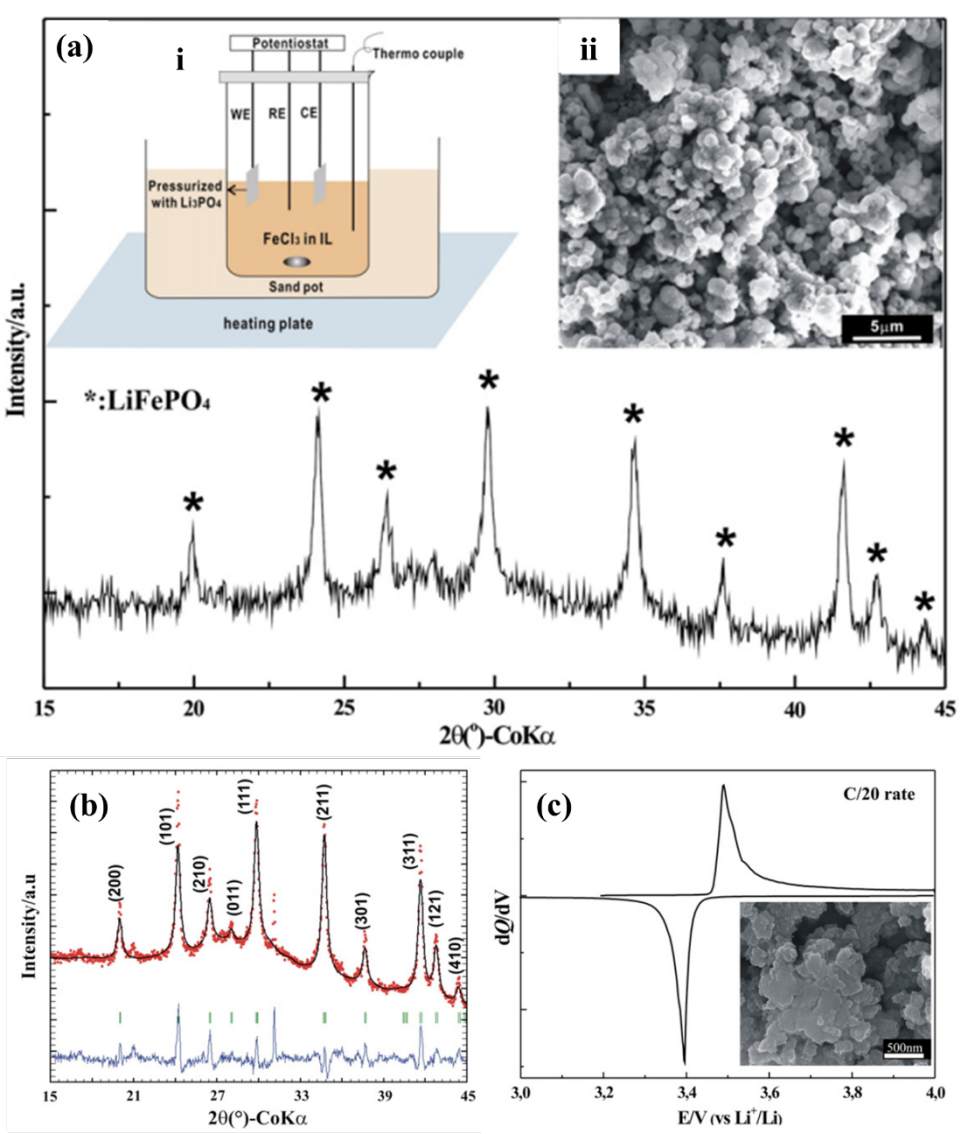


**Figure 4.** (a) XRD pattern of electrodeposited LFP film on Pt grid, (insets: (i) experimental setup of ECD and (ii) SEM image of LFP film prepared on Pt grid. (b) Rietveld refinement of the XRD pattern for LFP powder obtained under the optimized condition of ECD, and (c) dQ/dV charge-discharge plots of an electrode composed of the mixture of electrodeposited LFP powder with 15% Ketjen black at C/20 at 25 °C, (inset: SEM image of electrodeposited powder of LFP). Reproduced with permission from ref. [97]. Copyright 2011, Elsevier.

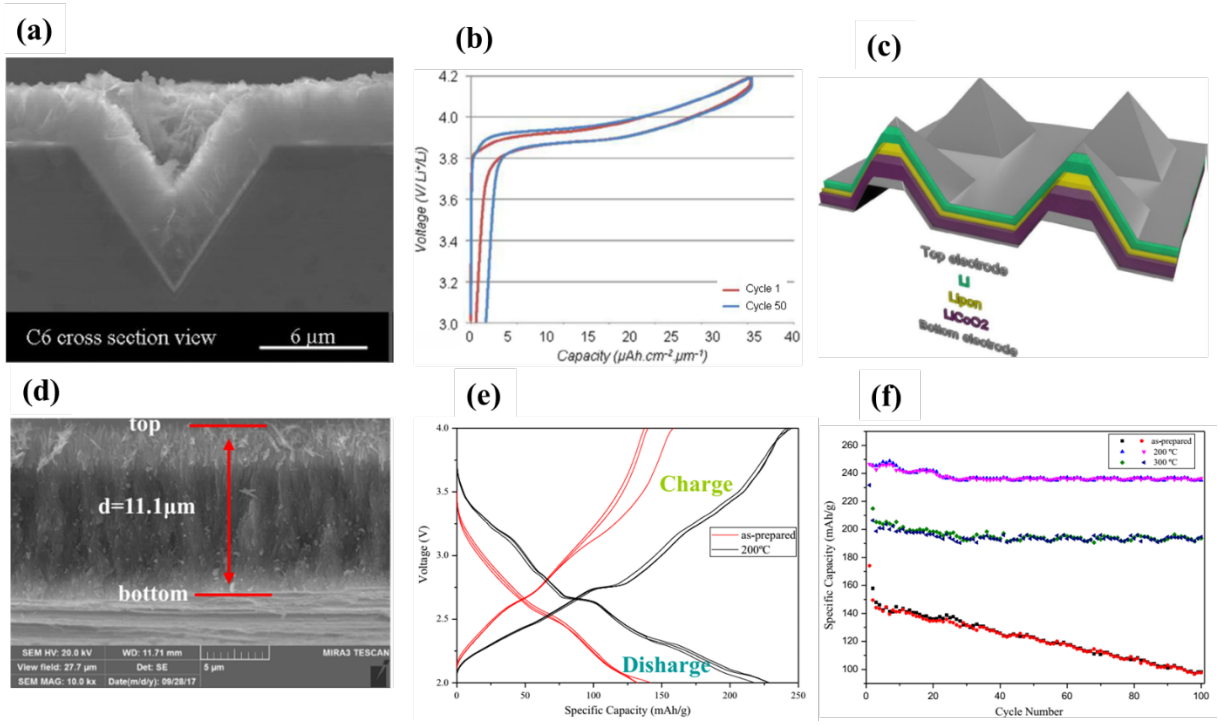


**Figure 5.** (a) SEM image cross-section view of LCO film deposited on the textured silicon substrate with a low aspect ratio of a rectangular pyramid. (b) The voltage-capacity profile of a 3D LCO 3D thin-film electrodeposited at 125 °C cycled at a constant current density of 30 µA.cm$^{-2}$. (c) Schematic illustration of a 3D microbattery using a stand-alone textured LCO electrode. Reproduced with permission from ref. [117]. Copyright 2016, Elsevier. (d) SEM image of the as-electrodeposited $Li_{0.04}V_2O_5$ on Ti foil (e) the voltage-capacity profiles of the as-prepared and annealed $Li_{0.04}V_2O_5$ films on Ti foil. (f) Cyclability of the as-prepared and annealed $Li_{0.04}V_2O_5$ films on Ti foil cycled at 30 mA g$^{-1}$. Reproduced with permission from ref. [123]. Copyright 2018, Elsevier.

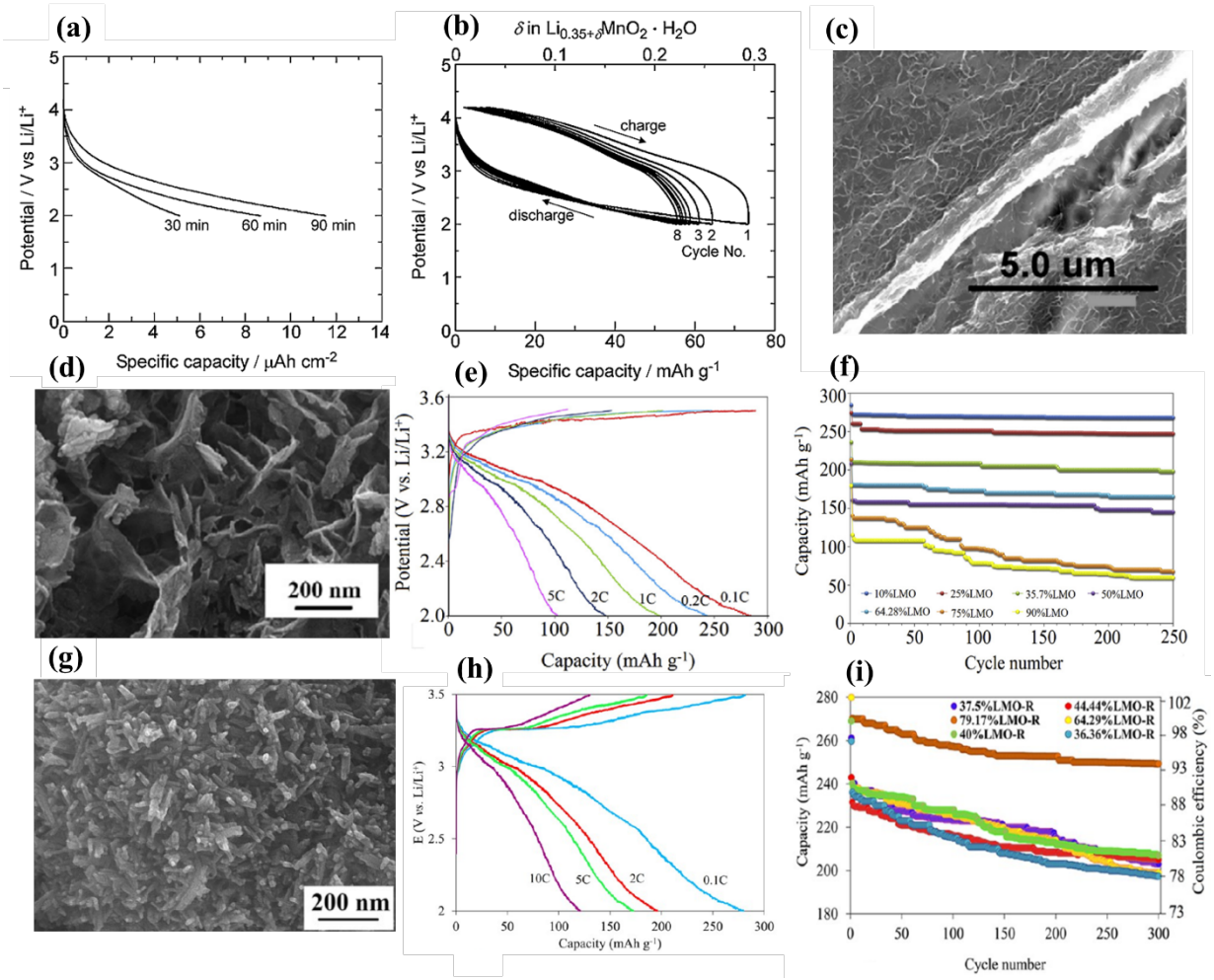


**Figure 6.** (a) Initial voltage-capacity profiles of $Li_{0.35}MnO_2.H_2O$ electrodeposited at different times. (b) voltage-capacity profiles of $Li_{0.35}MnO_2.H_2O$ electrodeposited in 60 min. (c) SEM image of the electrodeposited film of $Li_{0.35}MnO_2.H_2O$. Reproduced with permission from ref. [131]. Copyright 2008, Elsevier.(d) SEM image of the electrodeposited $Li_{0.41}MnO_2$ as a powder after scratching from the substrate. (e) The first voltage-capacity profiles of the electrodeposited $Li_{0.41}MnO_2$ using the pulse galvanostatic method at various C-rates within the range of 0.1 C−5 C. (f) Cyclic stability of the electrodeposited $Li_xMnO_2$ (x = 0.19 - 0.41) applying different values of the duty cycle of pulse current. Reproduced with permission from ref. [136]. Copyright 2018, Elsevier. (g) The SEM image of the electrodeposited $Li_{0.65}MnO_2$ as a powder after scratching from the substrate. (h) The first voltage-capacity profiles of the electrodeposited $Li_{0.65}MnO_2$ using pulse reverse galvanostatic method at various C-rates within the range of 0.1 C - 10 C. (i) Cyclic stability of the electrodeposited $Li_xMnO_2$ (x = 0.22 − 0.65) applying different values of the duty cycle of pulse reverse current. Reproduced with permission from ref. [137]. Copyright 2019, American Chemical Society.

1 **Table 1.** The electrochemical synthesis of Li-containing thin/thick film cathode materials of LIB/LIMB

| ECD media (electrolyte) | | ECD technique | Cathode material | Thickness (µm) | Electrochemical performance as cathode of LIMB/LIB | Ref. |
|---|---|---|---|---|---|---|
| **Molten salt** | (LiOH-KOH eutectic mixture)-CoO | Anodic Pulse potentiostatic at 260 °C | LCO | 25 | Specific capacity of 138 mAh $g^{-1}$ retaining 80% of the initial capacity after 400 cycles at 1 C | 76 |
| | | | | 100-130 | Specific capacity of ~ 160 mAh $g^{-1}$ at C/10, areal capacity of 9-12 mAh $cm^{-2}$ in LIMB (at 0.1 C for 3.0-4.3 V and 0.06 C for 3.0-4.7 V *vs.* $Li/Li^+$) | 88,89 |
| | (LiOH-KOH eutectic mixture)-MnO (~ 2Wt%) | | LMO | N/A | Specific capacity of 120 mAh $g^{-1}$, retaining 95% of the initial capacity after 400 cycles | 76 |
| | (LiOH-KOH eutectic mixture)-CoO-$Al(OH)_3$ | | Al-doped LCO | N/A | Specific capacity of 120 mAh $g^{-1}$ | |
| **Ionic liquid** | $FeCl_3$ and $Li_3PO_4$ in ionic liquid of [EMIm]TFSI | Potentiostatic at 275 °C | LFP | N/A | Charge and discharge peaks at 3.5 and 3.4 V *vs*. $Li/Li^+$ in dQ/dV curve | 97 |
| **Aqueous** | LiOH aqueous solution on Ni substrate | Anodic Galvanostatic-hydrothermal assisted at 150 °C for 20 h | $Li_{1-x}Ni_{1+x}O_2$ (LNO) | N/A | Oxidation and reduction peaks at ~ 4 V and ~ 3.3 V *vs.* $Li/Li^+$ | 100 |
| | LiOH aqueous solution containing cobalt metal powder | Anodic Galvanostatic-hydrothermal assisted at 100 – 200 °C for 24 h | LCO | 1.3 | Specific capacity of 35.4 µAh.$cm^{-2}$µ$m^{-1}$ at 10 µA $cm^{-2}$ , retaining 23% after 100 cycles | 110 |
| | $CoSO_4$ in LiOH aqueous solution | Anodic Galvanostatic at 120 °C for 30 min with capability of direct patterning | | N/A | N/A | 111 |
| | Leached liquor from the cathode of spent Li-ion batteries containing $Co(OH)_2$ and LiOH | Anodic Galvanostatic-hydrothermal assisted at 100 °C for 20 h | | 200 | Specific capacity of 127.1 mAh $g^{-1}$, retaining 97% of the initial discharge capacity after 30 cycles at 0.1 C | 112 |
| | LiOH, KOH solution and Co powder | Anodic Galvanostatic reflux method under ambient pressure at the temperature 150 °C for 8 h | | 12 | Specific capacity of 54.1 µA $cm^{-2}$ µ$m^{-1}$, at 10 µA $cm^{-2}$ retaining 85.6% after 15 cycles | 113 |
| | LiOH aqueous solution using Co substrate | Anodic Galvanostatic in sealed PTFE vessel at room temperature for 50 h | | 5 | Exhibiting a potential plateau at ~ 3.9 V *vs.* $Li/Li^+$ in 1.0 M $LiPF_6$/EC/DEC | 114 |
| | $Co(NO_3)_2$ in concentrated aqueous solution of LiOH | Anodic Galvanostatic-hydrothermal assisted at 150-200 °C for 1 h | | 6.5-6.8 | Electrodeposited LCO film at 200 °C retaining 90% after 50 cycles at C/5 | 115 |
| | 0.5 M $Co(NO_3)_2$ and 4 M LiOH in Wate/Ethanol solution | Anodic Galvanostatic-hydrothermal assisted at 125-200 °C | | ~4.5-28 | Specific capacity of ~ 80 mAh $g^{-1}$ at C/5 with fading capacity of -0.1% of initial capacity fades after /cycle for 130 cycles | 116 |

| | | | | | | |
|---|---|---|---|---|---|---|
| | $Co(NO_3)_2$ in aqueous solution of LiOH | Anodic Galvanostatic-hydrothermal assisted at 125°C for 1h | $Li_2Co_2O_4$ | ~ 2.6-5.0 depending on substrate | Specific capacity of 35 μAh $cm^{-2}$ $\mu m^{-1}$ at 30 μA $cm^{-2}$, retaining 80% of the initial capacity after 50 cycles | 117 |
| | The mixture of M $LiNO_3$ and $Co(NO_3)_2$ | Cathodic potentiostatic and subsequent transformation to $LiCo_2O_4$ under thermal annealing at 310 °C | | 1.2 | Specific capacity of 70 mAh $g^{-1}$ at 10 μA $cm^{-2}$ , retaining 67.5 mAh $g^{-1}$ after 50 cycles | 118 |
| | LiOH aqueous solution and vanadium plate | Anodic Galvanostatic-hydrothermal assisted at 150°C for 24 h | LVO | | N/A | 122 |
| | Aqueous solution containing $NH_4VO_3$, oxalic acid, hexamethylene tetramine, and $LiNO_3$ | Cathodic Potentiostatic under ambient pressure at 90 °C for 7 h | | ~ 11.0 | Specific capacity of 228.78 mAh $g^{-1}$ at 50 mA $g^{-1}$ after annealing at 200 °C | 123 |
| | Aqueous solution of $MnSO_4$ and $LiClO_4$ | Anodic potentiostatic for 1 h | $Li_xMnO_2$ ($Li_{0.35}MnO_2.H_2O$) | N/A | Specific capacity of 73 mAh $g^{-1}$ at 10 μA $cm^{-2}$ | 131,132 |
| | Aqueous solution of $MnSO_4$ and $LiSO_4$ | Anodic galvanostatic-at 80 °C | LMO (γ-$Li_{0.65}MnO_2$) | N/A | Specific capacity of 283 mAh $g^{-1}$, retaining 88% after 300 cycles at 0.1C | 137 |

**Table 2.** A summary of advantages and disadvantages of the various categories hitherto reported ECD of Li-containing cathode materials based on the electrolyte medium of ECD bath (i) molten salt reproduced with permission from ref.[76] Copyright 2017, Science (ii) ionic liquid[97] and (iii) aqueous medium Reproduced with permission from ref.[115]. Copyright 2011, Elsevier.

| i) Molten salt | | ii) Ionic liquid | | iii) Aqueous | |
|---|---|---|---|---|---|
| 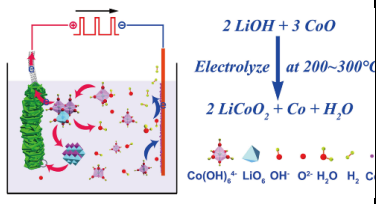 | | 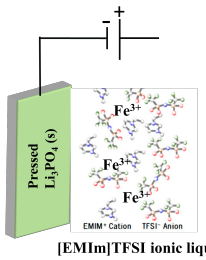 [EMIm]TFSI ionic liquid | | 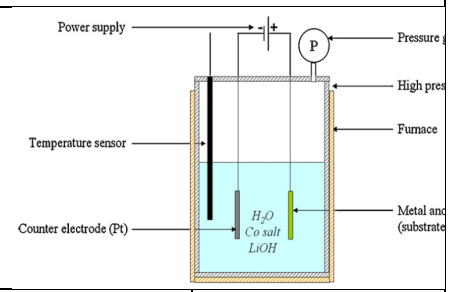 | |
| **Advantages** | **Disadvantages** | **Advantages** | **Disadvantages** | **Advantages** | **Disadvantages** |
| -Enabling conformal, monolithic and textured films (e.g., LCO with flexibility and preferred orientation of (110)[89])<br><br>-Intimate contact of the electrodeposited film with current collector<br><br>-Possibility of deposition on various substrates<br><br>-Good adherence and integrity of the film even at high thickness ranges of 200-500 µm[76]<br><br>-High density and mechanical stability of the electrodeposit | -Relatively high temperature<br><br>-Necessity of implementation under inert atmosphere | -Straightforward procedure<br><br>-One-step ECD with no requirement of post-annealing<br><br>-Higher sustainability compared to the other organic solvents | -Necessity of implementation under inert atmosphere<br><br>-Relatively high temperature<br><br>-Contamination of the electrodeposited materials (e.g., pressed solid $Li_3PO_4$ on the surface of the deposited LFP[97]).<br><br>-Relatively slow rate of ECD<br><br>-High viscosity of the electrolyte<br><br>-Precipitation of LFP in the solution alongside the surface of substrate | -The possibility of implementation under lower temperatures and non-inert atmosphere<br><br>-Straightforward and inexpensive procedure and equipment<br><br>-Fast deposition rate<br><br>-Enabling recovery of cathode materials from aqueous leached liquors (e.g., cathode materials from spent LIB as thin films[112]) | -Relatively poor electrochemical performance<br><br>-Deficiency of Li in the chemical composition especially for electrodeposited LMOs and LVOs<br><br>-High roughness and brittleness of the electrodeposited films<br><br>-Entailment of post-annealing to form electrochemically active phases especially in the case of LMOs and LVOs |

**Table 3.** A summary of the representative electrodeposited Li-free films as a cathode of LIB/LIMB

| Electrode material | ECD method | Set up and ECD bath | Post-annealing step | Electrochemical performance as thin-film cathode of LIMB/LIB | ref |
|---|---|---|---|---|---|
| **$MnO_2$** | Galvanostatic anodic method applying constant current within the range of 0.2-0.3 mA $cm^{-2}$ | Stainless steel or Ni plates as substrate and Pt counter electrode, bath containing 0.1 M $MnSO_4$ | - | Specific energy density = 580 Wh $kg^{-1}$, volume energy density = 2916 Wh $L^{-1}$<br>Cell consisting of $MnO_2$ thin film /$(PEO)_8LiClO_4$/Li delivered a volumetric capacity of 110 Ah $L^{-1}$. With a total thickness of cathode covered by electrolyte and anode of 3 µm and area of 1 $cm^2$. | 129 |
| **$MnO_2$** | Galvanostatic applying constant current within the range of 2-10 mA $cm^{-2}$ | planar Ti and 3D reticulated vitreous carbon as substates, Pt mesh as counter, and saturated $HgSO_4$ as a reference electrode in the bath containing 0.3 M $MnSO_4$ and 0.3 M $H_2SO_4$ | 400 °C under air for 5 h | Retaining 0.04 mAh $cm^{-2}$ after 100 cycles<br>On 2D planar Ti substrate<br>7 mAh $cm^{-2}$ on reticulated vitreous carbon as a 3D substrate | 77 |
| **$MnO_2$** | Galvanostatic anodic ECD at 0.5 mA $cm^{-2}$ on Ni-coated TiN substrate at 20-25 °C | A bath containing an aqueous solution of 0.3 M $MnSO_4$ and 0.3 M $H_2SO_4$ | 350 °C at $N_2$ atmosphere for 3 h | An areal capacity of 0.2 mAh $cm^{-2}$ at 20 C for the thin film with a thickness of 200 nm | 83,152 |
| **$V_2O_5$ (inverse opal)** | Potentiostatic ECD at 2.0 V vs SCE | Polystyrene coated stainless steel foil/FTO-ITO coated glass substrate as working electrode in a bath containing 0.25 M $VOSO_4.xH_2O$ solution in 1:1 vol/vol water/ethanol | 300 °C for 24 h | Specific capacity of 138.5 mAh $g^{-1}$ after the 2nd discharge, with delivering 82.1 mAh $g^{-1}$ at 0.6 C and 65.6 mAh $g^{-1}$ at 0.8 C and recovering 121.90 mAh $g^{-1}$ at 0.2 C | 84 |
| **$V_2O_5$** | Potentiostatic ECD at 2 V *vs*. SCE for 10 s | Si coupon with 10 nm Ti and 100 nm Au as a working electrode in a bath containing 0.25 M solution of VOSO4 in 1:1 vol/vol water/ethanol | Either annealing at 325 °C or drying by $N_2$ gun without annealing | A 3-electrode thin-film pouch cell LIMB using 0.25 µm thick film of Li foil and 1 $cm^2$ cathode in 0.5 M LiTFSI in C4mpyrTFSI delivering 120 mAh $g^{-1}$ at 0.75 C and rendering 110 mAh $g^{-1}$ at 2 C in the case of cycling with gel polymer electrolyte showing | 153 |

| | | | | | |
|---|---|---|---|---|---|
| | | | | capacity face 0.4% over 50 cycles at 5 C | |
| **$MoS_2/MoO_2S$** | Pulse current deposition | Using Ni-coated microchannel plate as working electrode and graphite as counter electrode in an aqueous solution of $Na_2S$ and $Na_2MoO_4$/PH = 7.5-8, in the presence of HCl and $KH_2PO_4$ | | 1 µm thickness of $MoS_2$-$MoO_2S$ on Ni coated glass microchannel plate-hybrid polymer electrolyte-lithiated graphite full cell 3D-LIMB delivering 2 $mAh.cm^{-2}$ retaining 60% of the capacity after 200 cycles for 100% DoD | [31] |
| **$MoO_xS_y$** | N/A | N/A | N/A | High energy $MoO_xS_y$ thin-film electrodeposited on a perforated substrate with 30,000 microchannels/$cm^2$ on 3D MB delivering 10 mAh $cm^{-2}$ which is stable over 500 cycles/high power $MoO_xS_y$ delivering 1 mAh $cm^{-2}$ which was stable over ~ 1200 cycles | [154] |
| **$MoO_xS_y$** | Sub-micron to several micrometers thick | N/A | N/A | Li ion/hybrid polymer electrolyte/$MoO_xS_y$ on Si on plannar configuration cycling at 100 µA $cm^{-2}$ for 1000 cycles with 0.02-0.06%/cycle and 100% Faradaic efficiency | [33,155] |
| **$FeS_2$** | Galvanostatic ECD on Ni substrate at 50 °C applying the current density of 1-10 mA $cm^{-2}$ | Bath containing an aqueous solution of $Fe_2(SO_4)_3$ and $Na_2S_2O_3$ and pH = 3.5-4.0 | 100 °C for 6 h under vacuum | Li/composite polymer electrolyte Li/(CPE)/$FeS_x$ at 50 µA $cm^{-2}$ and at 125 °C over 650 cycles showed 0,06%/cycle capacity fade and 100% Faradaic efficiency | [156] |

1